

EFFECT OF FUEL TEMPERATURE ON IN-NOZZLE CAVITATION AND SPRAY FORMATION OF LIQUID HYDROCARBONS AND ALCOHOLS FROM A REAL-SIZE OPTICAL INJECTOR FOR DIRECT-INJECTION SPARK-IGNITION ENGINES

P.G. Aleiferis*, J. Serras-Pereira and A. Augoye

Department of Mechanical Engineering, University College London, UK

T.J. Davies and R.F. Cracknell

Shell Global Solutions (UK), Ltd., Thornton, UK

D. Richardson

Jaguar Advanced Powertrain Engineering, Coventry, UK

*Author for Correspondence:

Dr. Pavlos Aleiferis

University College London

Department of Mechanical Engineering

Torrington Place, London WC1E 7JE, UK

Tel: +44-(0)20-76793862, Fax: +44-(0)20-73880180

E-mail: p_aleiferis@meng.ucl.ac.uk

Full length article accepted for publication in the International Journal of Heat and Mass Transfer

ABSTRACT

High-pressure multi-hole injectors for direct-injection spark-ignition engines offer some great benefits in terms of fuel atomisation, as well as flexibility in fuel targeting by selection of the number and angle of the nozzle holes. The flow through the internal passages of injectors is known to influence the characteristics of spray formation. In particular, understanding how in-nozzle cavitation phenomena can be used to improve atomisation is essential for improving mixture preparation quality under homogeneous or stratified engine operating conditions. However, no data exist for injector-body temperatures representative of real engine operation, especially at low-load conditions with early injection strategies that can also lead to phase change due to fuel flash boiling upon injection. This challenge is further complicated by the predicted fuel stocks which will include a significant bio-derived component presenting the requirement to manage fuel flexibility. The physical/chemical properties of bio-components, like various types of alcohols, can differ markedly from gasoline and it is important to study their effects. This work outlines results from an experimental imaging investigation into the effects of fuel properties, temperature and pressure conditions on the extent of cavitation, flash boiling and, subsequently, spray formation. This was achieved by the use of real-size transparent nozzles, replica of an injector from a modern direct-injection spark-ignition combustion system. Gasoline, *iso*-octane, *n*-pentane, ethanol and butanol were used at 20, 50 and 90 °C injector body temperatures for ambient pressures of 0.5 bar and 1.0 bar in order to simulate early homogeneous injection strategies for part-load and wide open throttle engine operation. The fuel matrix also included a blend of 10% ethanol with 90% gasoline (E10) because the vapour pressure of E10 is higher than the vapour pressure of either ethanol or gasoline and the distillation curve of E10 reflects strongly this effect. Therefore, the distillation curves of the fuels, the vapour pressures, as well as density, viscosity and surface tension were obtained and the Reynolds, Weber, Ohnesorge and Cavitation numbers were considered in the analysis. The in-nozzle flow regime and spray formation was found to be sensitive to the fuel temperature and gas pressure as a result of the vapour pressure and temperature relationships.

NOMENCLATURE

Ca	Fluid Dynamics Cavitation Number
CN	Pressure Ratio Cavitation Number
d	Diameter
L	Length of Nozzle Hole
μ	Dynamic Viscosity of Liquid
ρ	Density
p	Pressure
p_{∞}	Reference Pressure
p_g	Gas Pressure
p_{inj}	Injection Pressure
p_v	Vapour Pressure
Re	Reynolds Number
σ	Surface Tension
T	Temperature
T_{∞}	Reference Temperature
u	Velocity
U_{∞}	Reference Velocity
W	Width

ABBREVIATIONS

ASTM	American Society for Testing and Materials
CAD	Computer Aided Design
DISI	Direct Injection Spark Ignition
DVPE	Dry Vapour Pressure Equivalent
RPM	Revolutions Per Minute

INTRODUCTION

INJECTORS AND CAVITATION

When heat is supplied to a liquid at a constant pressure, after a period of time, the liquid experiences a phase change into vapour. When this occurs, the liquid is said to have undergone boiling. In contrast, when phase change occurs as a result of pressure drop of the flowing liquid at a constant temperature, cavitation is said to have taken place. Cavitation is a phenomenon that is mainly encountered in hydraulic equipment such as hydro-turbines, pumps, valves and ship propellers where hydrodynamic effects result in regions of flow experiencing a pressure which falls below the vapour pressure of the liquid at that particular temperature, causing the formation of bubbles or foam at suitable nucleation sites. In a hypothetical flow where the liquid cannot resist any tension, vapour bubbles would appear immediately when the pressure reached the vapour pressure. However, nucleation does not typically happen instantaneously due to varying levels of nuclei present in the test liquid (*e.g.* from contaminant gas or otherwise) and the fact that growth rates are finite, requiring a certain ‘residence time’.

Cavitation phenomena have been known to occur inside Diesel injectors for the past 50 years or so [1]. Cavitation can occur at the centre of vortices in a flow due to centrifugal static pressure differentials; vortical motion can occur not only because it is inherent in turbulent eddies but also because of the presence of both free and forced shedding vortices. This is particularly relevant inside injector nozzles where the flow can have vortex motion by design, *e.g.* rotational/swirling flow patterns upstream the nozzle hole, and/or because the flow must turn round sharp radii, *e.g.* at the inlet of the nozzle which can result in significant recirculation zones just downstream the inlet of the nozzle. Although cavitation is not desirable on many occasions since the collapse of the cavitation bubbles can have a negative effect on the mechanical integrity of the interacting components through surface erosion, cavitation in injection nozzles is recognised as a phenomenon that can be beneficial to the development of the fuel spray. This is due to the fact that the primary break-up and subsequent atomisation of the liquid fuel jet at the nozzle exit can be improved by the perceived disruption of the flow and enhanced turbulence caused by the cavitation patterns within the flow [2]. In addition, the dynamics of cavitation inside the nozzle is expected to enhance fuel atomisation through generation of smaller droplets which vaporise more rapidly, thus enhancing the fuel/air mixing and reducing ignition delay in Diesel engines.

Multi-hole Diesel injector technology has illustrated the benefits of increasing fuel pressure on atomisation and this has led to the development of multi-hole injectors for gasoline Direct-Injection Spark-Ignition (DISI) engines. A multi-hole injector for DISI engines allows fuel to be injected through a number of small holes in the injector tip, whose position and angle can be varied in any required configuration to direct the fuel towards the spark plug or any other in-cylinder area of interest. This has led to the so-called ‘spray-guided’ combustion system that has become the preferred choice for DISI engines due to demonstrated stability of performance under a wide range of operating conditions [3].

Most previous studies on multi-hole injectors have focused on cavitation imaging in optical models of scaled-up Diesel nozzles, with few studies on real-size nozzles and, moreover, with only limited work on

quantitative flow data in scaled-up or real Diesel injectors, *e.g.* by Aleiferis *et al.* [4] in a 20× model and by Tropea and co-workers in a real-size geometry [5, 6]. Research conducted in some real-size and model injectors with optical access has questioned the direct scaling of cavitation phenomena in injectors even when relevant non-dimensional parameters been matched on models. In one of the earliest studies on injector nozzles, Bergwerk [1] conducted experiments with simplified large scale-and real-size single-hole Diesel nozzles and observed that for the large-scale nozzle, increasing cavitation continuously led to a transition into hydraulic flip; on the contrary, increased cavitation brought about a more atomised spray. In a much later study, Arcoumanis *et al.* [7] made a critical comparison between large-scale and real-size Diesel nozzles and found that cavitation in models occurred in the form of foamy clouds of bubbles, similar to those of Soteriou *et al.* [8]; in real-size injectors though, cavitation appeared in the form of large clear voids, similar to those of Chaves *et al.* [9]. These results suggest that the nature of cavitation inception may change in scaled-up models and that bubble scaling factors are still not well understood.

The different operating conditions of DISI engine injectors to those of Diesel engines highlight the importance of undertaking studies of fuel flow inside the nozzles of DISI injectors for a better understanding of their spray formation and mixture preparation characteristics. Previous studies of flow and cavitation in gasoline injectors are very few and have focused on scaled-up models, *e.g.* in a 10× model by Aleiferis *et al.* [10], or on single-hole pressure-swirl atomisers [11–14]. In general, cavitation was always found to produce a more broken-up spray; however, in extreme cases examined by Allen *et al.* [12] in pressure-swirl atomisers, cavitation filled the entire nozzle resulting in hydraulic flip which effectively reduced the atomisation ability of the nozzle. The rapid transitions from the initial onset of cavitation to the complete saturation of the nozzle showed the process to be highly unstable and difficult to control. Recently, Gilles-Birth *et al.* [15, 16] investigated the effect of cavitation in multi-hole DISI injectors. They used a real injector coupled to a real-size optical nozzle with a single angled orifice 0.2 mm in diameter. They identified three types of cavitating structures: bubble, film and string cavitation. The latter was found for nearly all operating conditions and started at the injector needle due to strong rotational flow at the nozzle inlet, growing towards the nozzle exit but was very unstable in its development, shape and shot-to-shot repeatability. Film cavitation and supercavitation were the dominant modes, the former observed to have stronger regions on the top side of the nozzle as bubbles were created at the nozzle inlet and flushed away and the latter used to define conditions where bubbles completely filled the nozzle.

All previous experiments of cavitation in injections nozzles, particularly of multi-hole design, have been conducted at fixed temperature and with fixed liquids. In fact, several different liquids that have been used for such investigations include Diesel oils, calibration oils, unspecified hydrocarbon mixtures, white spirits and gasolines, all of which have widely different transport properties such as surface tension (σ), viscosity (μ), density (ρ), boiling point and vapour pressure (p_v). A major challenge in scaling is how to anticipate cavitation in one liquid, based on data obtained from another; since nuclei play an important role, scaling from one fuel to another would only be tentative, especially in the context of realistic engine operating conditions. More to the point, DISI injectors are mounted in an engine head where the fuel inside the injector

and the spray upon injection are both subjected to a wide range of conditions. For example, DISI injectors must inject fuel at conditions of low ambient pressure, typically from ~ 0.2 bar at low load with early injection strategies for homogeneous mixture formation, to ~ 5 bar for late-injection strategies under stratified engine operation, or even more under supercharged operation. Additionally, fuel temperatures can vary from below $0\text{ }^{\circ}\text{C}$ to over $150\text{ }^{\circ}\text{C}$ at the injector tip under high-load firing conditions. Although quite significant phenomena are coupled over this operation regime, very few experimental results exist to explain such effects in multi-hole type DISI engine nozzles. Specifically, for the case of low-load operation with fully-warm engine conditions, fuel flash-boiling occurs as there is fast disruptive evaporation of the fuel upon injection due to the reduction of the fuel's boiling temperature from the rapid depressurisation into the engine cylinder. This enhances the rate of evaporation but also leads to 'spray collapse' that draws the plumes close together under the injector tip and destroys the designed directionality of the plumes. It is very likely that over this regime, in-nozzle phase-change phenomena due to cavitation get immediately coupled to phase-change phenomena arising from boiling, altering the spray formation in a complex, currently unknown, manner. This mechanism can be better analysed with investigations using optical nozzles. Experimental results on the subject can also assist researchers in the area of computational fluid dynamics because although some models have been developed to predict cavitation and its effect on sprays, only models of limited applicability exist for multi-component fuels, especially at high fuel temperature and low gas pressure flash-boiling conditions.

SPARK-IGNITION ENGINES AND BIOFUELS

The challenge is further complicated by the predicted fuel stocks which will include a significant bio-derived component in order to strengthen sustainability and reduce CO_2 emissions, presenting the immediate requirement to manage fuel flexibility. In the short term we need to ensure the bio-components are compatible with modern engines and to determine appropriate blend formulations. Understanding the effect of new bio-components on fundamental engine processes, such as spray formation, is an essential part of this challenge, especially in DISI engines that are very sensitive to fuel properties. Gasoline already contains 5% bio-ethanol (E5) in many countries and is compatible with existing combustion systems but its use will have only limited impact on CO_2 emissions. Ethanol increases the octane rating of the fuel. This allows a more optimised spark timing in current vehicles and permits higher compression ratios to be employed in future engines, giving rise to higher thermodynamic efficiency. The high flame speed of ethanol and charge cooling benefits effects may also increase the thermodynamic efficiency, depending on the spark timing and injection strategy. There is pressure for the ethanol content of fuels to increase with some markets demanding much higher proportions (E85 or E100). The vapour pressure of an E5 or E10 blend is higher than the vapour pressure of either ethanol or gasoline as the mixture deviates from the ideal solution behaviour (Raoult's law) due to the intermolecular forces. This deviation from Raoult's law significantly alters the distillation curve of the blend in comparison to that of pure gasoline [17, 18]. For E100 certain issues can also arise at cold-start engine conditions due to the lack of volatility, but this is not a problem for E85. The chemistry of ethanol is very different from that of hydrocarbon fuels. For one thing ethanol is water soluble which necessitates rigorous procedures during fuel distribution. Additionally, not all components on the vehicle

which are compatible with hydrocarbons would necessarily be compatible with blends containing large amounts of ethanol. The volumetric energy density of ethanol is also lower than gasoline which poses a challenge for the engine calibrator in terms of controlling the injector pulse width. Other alkyl alcohols, such as butanol have also been suggested as possible gasoline components. Having twice as many carbon atoms as ethanol, butanol is more hydrocarbon-like in its properties. However butanol lags far behind ethanol in terms of commercial production.

PRESENT CONTRIBUTION

There are still limited experimental data which clarify the role that liquid transport properties, such as surface tension, viscosity, density, boiling point and vapour pressure, have on in-nozzle phenomena and overall spray development over a realistic range of DISI engine operating conditions. Analysis of the Cavitation, Reynolds and Weber numbers is significant in atomisation systems, but such non-dimensional parameters have yet to be characterised and studied fully in the context of DISI engine injector nozzles with traditional and alternative fuels that have different properties. There are also no experimental results of the interactions between cavitation and flash-boiling at extremes of pressures and temperatures using real-size optical nozzles with various types of fuels. Therefore, the main objective of this work was to investigate such effects for different fuels and conditions. This was achieved using real-size optical nozzles to simulate the flow in one of the holes of a real multi-hole injector used recently by the authors for macroscopic spray imaging and related engine studies [3, 19–23]. Specifically, two transparent real-size single-hole nozzles with different nozzle-hole diameters and lengths were developed and coupled to a real injector body that was mounted on a quiescent pressure chamber to allow simulation of typical DISI engine operating conditions. A series of experiments were conducted for visualization of the cavitation inside the injector nozzle and the resulting effect on spray development. The investigation was carried out for gasoline, *n*-pentane and *iso*-octane, as well as ethanol, butanol and E10, over a range of chamber pressures and fuel temperatures.

EXPERIMENT APPARATUS AND PROCEDURE

PRESSURE CHAMBER

Cavitation and its effect on near nozzle spray were investigated using back lighting visualization. All fuel injection events were conducted in a quiescent pressure chamber. Its octagonal shape and its six optical windows enable simultaneous multi-technique characterisation such as imaging with back lighting or side lighting, and the use of off-axis techniques for droplet sizing and velocity measurements. Figure 1 shows picture of the pressure chamber. The chamber pressure was monitored by an absolute pressure sensor mounted in the lid of the chamber. The chamber's gas temperature was monitored throughout the experiment by a K-type thermocouple mounted in the lid of the chamber with the sensing tip located near the injector mounting. A valve at the bottom of the pressure chamber enabled evacuation of liquid and vapour fuel as well as creating sub-atmospheric pressure within the chamber through its connection to a vacuum pump system. The chamber windows in the axis of imaging were regularly removed and cleaned for better image visualization. More details about the chamber can be found in [21].

INJECTOR

A multi-hole injector originally designed for vertical installation in a DISI engine head in close spacing arrangement with the spark plug of a gasoline engine was used for this investigation. The injector had six nozzle holes in an asymmetric arrangement with different angles with respect to the vertical axis. Figure 2 shows a schematic of the injector and its spray plumes through two views. Plumes 1 and 6 had a 58.5° inclination with respect to the vertical axis and have been designed to pass on either sides of the spark plug *i.e.* one at the intake side and the other at the exhaust side of the engine. More details about the injector geometry, nozzle-hole angles and spray formation in a quiescent environment and in a running DISI engine can be found in previous studies by the current authors [3, 19–23]. The injector was fitted into a specially designed mount positioned at the centre of the upper lid of the pressure chamber. A band heater was attached to the injector to heat up its body temperature, replicating *in-situ* heating of injectors mounted in DISI engine heads. A thermocouple sensor provided feedback to a temperature controller which regulated the injector temperature as required by each experiment. The temperature measured was that of the injector body, as this was the best possible arrangement in obtaining the fuel temperature using the available apparatus. As a result of this, each time the system was heated to a particular test temperature and the temperature was held constant for an hour, allowing enough heat-soak for a uniform distribution of temperature within the whole injector mount mass, before spray imaging was conducted. More details about the injector mounting and heating arrangement can be found in previous studies [21–23]. In order to replicate in-cylinder injection conditions flow imaging was carried out with the injector housing at 20°C and heated to temperatures of 50°C and 90°C to simulate engine conditions from cold-start to fully warmed-up. Both atmospheric (1.0 bar) and sub-atmospheric (0.5 bar) gas conditions were investigated to simulate ‘full-load’ and ‘low-load’ engine operation with early injection strategies, *i.e.* with start of injection during the early part of the intake stroke for homogeneous mixture formation. The gas temperature was monitored at 20°C throughout each experiment.

OPTICAL NOZZLE

For in-nozzle cavitation investigations, optical nozzles were manufactured from Perspex[®] and coupled to the body of the real injector described above and used for all investigations. The sides of the nozzle stem were made flat to avoid refraction of imaged light during the experiment. The refractive index of Perspex[®] is 1.495 and the melting point typically in the range $90\text{--}115^\circ\text{C}$ ($363\text{--}388\text{ K}$).

The real injector was disassembled, revealing the internal needle and a specially designed adaptor, manufactured from steel, was used to couple the optical nozzle to the real injector body. This assembly is illustrated in Figure 3 in four phases ending with the injector as mounted in the pressure chamber with a ‘blank’, *i.e.* non-drilled, optical nozzle. The internal geometry of the real injector was analysed to obtain realistic optical geometries for the investigation. Critically, it was found that although the external diameter of all nozzle holes was 0.5 mm, there was step change of the nozzle diameter inwardly and the internal diameter was 0.2 mm. This step change was designed to avoid deposit formation. In summary, the inner hole

diameter was 0.2 mm with length ~ 0.25 mm and the outer hole diameter was 0.5 mm with length ~ 0.25 mm, leading to a total nozzle hole length of 0.5 mm.

The study of cavitation reported in the current paper used two optical nozzles that were designed for simultaneous imaging of both the nozzle flow and the resulting spray. In an initial attempt to avoid the exact complexity of the real injector, and considering cautiously the properties of the optical material, the first nozzle (Nozzle A) had a diameter of 0.5 mm and a length of 2.5 mm (giving $L/d=5$). The second nozzle (Nozzle B) was an evolution of the first design, allowing a diameter of 0.2 mm and a length of 1.0 mm (giving again $L/d=5$) and a lower position closer to the bottom of the needle seat, for a more faithful representation of the real injector. The hole was designed at 60° angle to the vertical for both nozzles as an approximate to 58.8° of plumes 1 and 6 of the real injector shown earlier in Figure 2. Figure 4 shows CAD drawings of the two optical nozzles.

The fuel injection pressure was supplied by a pneumatic-piston ram pump. The pump was powered by compressed air flowing through an automatic shutoff and release system which could be depressurised using an electric shut-down button when necessary. A flexible hose was used to connect the output of the pump to an injector. Just before the injector, there were a bleed valve, a pressure gauge, a safety valve and a solenoid valve that was used to trigger the injection event from the control room. Due to the material properties of the optical nozzle, the injection needle was stationed in a constantly open position, allowing injection event to be controlled using the solenoid valve. This was done to prevent the needle seat from wearing caused by the steel needle making forceful contacts with the optical material, especially at the high fuel temperatures. It is also worth noting that the optical nozzle required continuous cleaning; in fact, this had to be done after every single injection event, to avoid distortion of images from refraction of light rays by fuel films on the optical nozzle body.

CAVITATION AND SPRAY VISUALIZATION SETUP

High magnification imaging of the nozzle and spray was conducted with a Photron[®] APX high-speed digital video camera. The camera was set to a frame rate of 9000 frames per second (corresponding to 1° crank angle resolution for an engine running at 1500 RPM) and a pixel resolution of 640×480 . A Model K2/SC[™] series long-distance microscope system from INFINITY was used to obtain suitable magnification for imaging simultaneously the in-nozzle cavitation and outer spray formation. For all measurements, back-lighting was provided by a photographic flash lamp. The spark flash light was of 4 ms duration and was diffused through a semi-opaque optical sheet to provide uniform background. Camera shutter speed was set to $1/50,000$ second to allow several ‘frozen’ images to be acquired over the flash duration. Figure 5 shows a schematic representation of the experimental setup. The high speed camera was connected via a fire-wire cable to a computer where images were recorded and displayed. Triggering of the high speed camera, flash lamp and solenoid valve was provided by an AVL 327 engine timing unit. Since the injector needle was constantly in a position of full lift as explained earlier, injection triggering was performed solely by the solenoid.

FUELS

Six fuels were investigated: a typical commercial grade gasoline (RON95), *iso*-octane, *n*-pentane, butanol, ethanol and E10 (blend of 10% ethanol with 90% gasoline). The distillation curves of all fuels are shown in Figure 6. A standard commercial grade European gasoline contains several hydrocarbons typically about 35–40% C5 or lower (including oxygenates), similar levels of C6–C8 and the remainder C9–C10 hydrocarbon chains. *Iso*-octane is a single component of gasoline with boiling point temperature of 99 °C at atmospheric pressure while *n*-pentane, also a single component of gasoline, boils at 36.1°C. *Iso*-octane and *n*-pentane were investigated to ascertain the effects of fuel constituent properties on in-nozzle phenomena of gasoline as well as to aid interpretation of results obtained using the standard gasoline. Butanol boils at 117°C while ethanol boils at 78.4°C. E10 was selected because the vapour pressure of E10 is higher than the vapour pressure of either ethanol or gasoline. The main reason for this is that the mixture deviates from Raoult's law due to the intermolecular forces, and the distillation curve in Figure 6 reflects clearly this effect. More information about this and other ethanol-gasoline blends can be found in [17, 18]. Finally *o*-xylene, a heavier gasoline component with boiling temperature 144 °C was considered and has been included in Figure 6, as well as in subsequent various plots to aid results discussions but was not included in the test matrix because its properties make it quite insensitive to the phenomena being investigated. This component served only to define the range of gasoline's thermo-physical properties, which is useful when discussing the effects of different chemical components on the observed behaviour of gasoline as a multi-component fuel.

More information about the physical properties of gasoline and some of the other fuels that were tested for the current study can be found in previous publications by the current authors, *e.g.* see [20–23]. The vapour pressure curves of all fuels tested are shown in Figure 7. The vapour pressures for *iso*-octane, *n*-pentane, *o*-xylene, ethanol and butanol were calculated using correlations obtained from [24] within a valid temperature range. For gasoline and E10 the vapour pressures were obtained experimentally using ASTM D5190 (Dry Vapour Pressure Equivalent, DVPE) at Shell Global Solutions (UK), Ltd.

Clear imaging of in-nozzle phenomena depends on the closeness of the refractive index of the fuel to that of the nozzle's optical material. The refractive index of each of the fuels at 25 °C (298 K) is: gasoline 1.427, *iso*-octane 1.388, *n*-pentane 1.358, ethanol 1.362, butanol 1.395, and drops by about 1.4–1.7% when fuel temperatures go to 90 °C (363 K).

RESULTS AND DISCUSSION

NON-DIMENSIONAL PARAMETERS

Images of spray development, including near-nozzle spray characteristics, using the multi-hole injector of the current publication, have been presented in recent papers by the current authors [21–22]. Features of the primary spray break-up and the macroscopic spray formation brought about by changes in the operating conditions, namely spray convergence and collapse at high fuel temperatures and low gas pressures due to flash boiling, were discussed for various types of gasoline and the single-components *n*-pentane and *iso*-octane. The reader might find these useful to bring the current publication into context.

The spray characteristics of injectors depend not only on the physics of atomisation of the liquid jet but also on the levels of turbulence generated by the internal flow upstream of the nozzle exit, as well as the extent to which cavitation occurs inside the nozzle passage. Decoupling these competing effects is not trivial and non-dimensional parameters can provide some assistance.

The effect of turbulence can be characterised by the Reynolds number $Re = \rho ud/\mu$ where ρ and μ are the density and dynamic viscosity of the liquid fuel, respectively, d is the nozzle hole diameter and u the flow velocity in the nozzle.

The Cavitation number, Ca , is typically used to characterize the sensitivity of a flow to cavitation and is defined as:

$$Ca = \frac{p_\infty - p_v}{\frac{1}{2}\rho U_\infty^2} \quad (1)$$

where p_∞ is the pressure at a reference point in the flow, p_v is the vapour pressure of the liquid at the reference temperature T_∞ , ρ is the liquid density and U_∞ is the characteristic velocity at the reference point. All flows will have some value of Ca whether cavitating or not. At large values of Ca , flows will be single-phase due to either p_∞ being very large compared to p_v or the flow velocity U_∞ being very small. As the Cavitation number decreases however, nucleation will first occur at some value of Ca dependent on experimental conditions and fluid properties. This is usually denoted as incipient cavitation and defined by a critical Cavitation number Ca_{cr} . Further reduction in the Cavitation number below this value will cause an increase in the number of vapour bubbles. The rate growth of bubbles is radically affected by the thermodynamic properties of the liquid and vapour which are functions of temperature; therefore, Ca_{cr} will also depend on the liquid temperature.

A range of critical Cavitation numbers which define the cavitating transition have been quoted in the literature relating to Diesel injectors for a variety of nozzle-hole geometries and injection parameters. However, the most popular definition of a Cavitation number for injection phenomena has not been that shown in Eq. (1) but the following:

$$CN = \frac{P_{inj} - P_g}{P_g - P_v} \quad (2)$$

where p_{inj} is the injection pressure, p_g is the gas pressure and p_v is the vapour pressure. This is not strictly correct from a fluid dynamics perspective but makes comparisons with data from different experimental arrangements simpler, since the effect of flow velocity is eliminated and only experimental conditions relating to injection, gas and vapour pressures are considered, *i.e.* the ratio of forces that support versus those that suppress cavitation. Critical Cavitation numbers based on this definition, *i.e.* CN_{cr} , have been found to fall in the range of 0.5 to 10, with associated Re_{cr} of between 5,000 and 30,000 [1, 2, 11, 13 15, 16, 25]. Once in the cavitating flow regime, the discharge coefficient of the nozzle is mainly dependent on CN and independent of Re .

This analysis implies that the cavitation and Reynolds numbers should be controlled as much as possible in cavitation experiments. Obviously this is not trivial, especially when considering modifications to a system for optical access which might involve some change in configuration or scale. For example attempts to match Re by changing the flow rate on a large-scale model may lead to confusion due to effects on the residence time and the Cavitation number. The pressure can be changed to recover the Cavitation number but this can then alter the nuclei content. Additionally, fluid transport properties have different non-linear temperature and pressure dependencies, therefore, the use of a global transition regime map from non-cavitating to cavitating flows is difficult to build up. On a positive note, however, the above parameters are all much less sensitive when cavitation is already developed, justifying the continued use of Re and the Cavitation number as the two most widely used non-dimensional parameters for such studies.

For consistency between the real injector and the optical nozzles, flow rate measurements were conducted in order to match the Reynolds number Re of the real injector and the optical nozzle. The injector flow rate was measured while injecting at a constant working pressure of 150 bar. This was divided by the number of nozzle holes (six) so as to obtain the flow rate per nozzle. The flow rate of real injector at 150 bar injection pressure was 16.68 g/s giving an approximate flow rate of 2.78 g/s per nozzle. Injection pressure was varied while injecting through the optical nozzle, and an injection pressure of 23 bar gave a flow rate of 2.81 g/s which closely approximated that of the real injector. Hence all injection events using optical Nozzle A were carried out at 23 bar. The jet velocity was obtained by dividing the nozzle mass flow rate by the product of the fuel density and the flow area using a diameter of 0.5 mm. This was calculated to be 22 m/s. Nozzle B has a hole diameter of 0.2 mm. An injection pressure of 40 bar was found to give the same Reynolds number to the real injector and Nozzle A. The velocity of the jet from Nozzle B was calculated to be 55 m/s.

Figure 8 shows the Re plot for all single-component fuels tested with fluid properties of density and viscosity for varying temperatures along the liquid saturation curve. Measurement of the viscosity of multi-component fuels like gasoline or E10 are not trivial to make consistently over a range of varied temperature and pressure conditions necessary for constructive analysis and such measurements were not made available for these two specific fuels tested. Therefore, in Figure 8 the shown reference single components *n*-pentane, *iso*-octane and *o*-xylene are used to define the general envelope of gasoline's multi-component nature. In the range 20–90 °C, the calculated Re numbers were 4,000–40,000; interestingly, butanol's Re at 20 °C was the lowest, indicating flow very close to laminar conditions.

The Cavitation numbers Ca and CN are shown in Figures 9–11 for all the single-component fuels tested; Figure 9 also contains gasoline's Ca at 20 °C (293 K) where the density of gasoline was available, whilst Figure 10 and 11 also contain gasoline's and E10's CN over the temperature range where vapour pressure data were available from Figure 7. It can be observed that the Cavitation numbers Ca obtained from Eq. (1) (with p_∞ set to p_{inj} and U_∞ set to the flow velocity in the nozzle u) are smaller in magnitude when compared to CN obtained from Eq. (2). Also, there is an approximate constant increase in Ca with temperature against the continuous change in the slope of CN . The effect of temperature on Ca is relatively small, with Ca increasing by ~10% when temperature increases from 20 °C (293 K) to 90 °C (363 K); this increase comes

essentially from the effect of density in the denominator of Eq. (1) because the numerator decreases drastically with temperature from the effect on the vapour pressure (Figure 7). Concerning CN , the effects of temperature on vapour pressure shows vapour pressure increasing with temperature therefore causing the denominator of CN to approach a negative value, leading to negative values of Cavitation number. Hence only values up to the transition point from positive to negative Cavitation number have been plotted for clarity. It can further be observed in Figures 10 and 11 that CN values are considerably lower at the higher gas pressure. One important observation in the Cavitation number that needs to be highlighted is the trend for gasoline which appears to be more temperature sensitive in comparison to *iso*-octane. Although *iso*-octane is commonly used as a substitute for gasoline in many engine research applications, Figure 7 and pictures obtained from macroscopic imaging of the real multi-hole injector, *e.g.* [21], shows that higher volatility components, like *n*-pentane, are better substitutes for gasoline when a single-component fuel is to be used to model gasoline especially at elevated temperature conditions. This is particularly important to spray modellers who are normally faced with modelling a complete gasoline blend and have to make decisions on which single components might be more appropriate to use.

The atomisation process can be described by Re and the liquid Weber number $We = \rho u^2 d / \sigma$, where u , d , ρ and σ are a characteristic velocity, a characteristic diameter, the liquid density and surface tension, respectively. Alternatively, the Ohnesorge number $Oh = We^{0.5} / Re$ may be used which incorporates all the main fluid properties. Therefore, proper study of the effect of cavitation on atomisation requires simultaneous matching of We . By matching Re between the real ‘full-metal’ multi-hole injector and the real injector with the optical nozzle, a Weber number based on the nozzle diameter d and the flow velocity u in the nozzle as measured for Re is also matched. Following this process, comparisons can be performed between the cavitation and spray images of different fuels at different conditions of temperature/pressure where the Cavitation numbers and/or We are similar.

Figures 12 and 13 present the calculated We and Oh numbers for the single components selected and for temperatures from 7 °C (280 K) up to 185 °C (458 K) and for both nozzles. The Ohnesorge [26] diagram is shown in Figure 14 for the same components, with the Reitz and Bracco [27] break-up regimes superimposed. It is quite interesting that *n*-pentane is generally in the atomisation regime when used with both nozzles but *iso*-octane lies in the atomisation regime only with Nozzle B and crosses into the second wind induced regime when it is colder than ~70 °C (343 K) with Nozzle A. The heavy component of gasoline, *o*-xylene, crosses into the second wind induced regime when it is colder than ~100 °C (373 K) and ~40 °C (313 K) with Nozzles A and B, respectively. The two alcohols lie mostly in the second wind induced regime and cross into the atomisation regime only when at quite high temperatures and this is quite interesting in its own right considering the implications for engine cold-start conditions. Specifically, butanol crosses into the atomisation regime only when hotter than ~120 °C (393 K) and ~80 °C (353 K) with Nozzles A and B, respectively, whilst ethanol only when hotter than ~100 °C (373 K) and ~50 °C (323 K), respectively. Similar observations can be drawn from the We diagram in Figure 12. Most values for alcohols

lie well below the atomisation regime defined as $We > 30,000$ by Sallam *et al.* [28] who used non-cavitating water and ethanol sprays in their experiments.

Transition criteria based on Re or We numbers are not easy to find in the literature for similar jet and operating conditions, particularly with real fuels. Some experiments with similar magnitudes of Re and We to those of the current study were performed by Suh and Lee [29] on two-dimensional nozzles with dimensions 5×2 mm and length to width ratios (L/W) of 1.8 and 2.7, *i.e.* with the latter similar to the injector nozzle of the current study, using Diesel fuel but critically under turbulent to cavitating transition conditions. Transition criteria were established by these authors for turbulent to cavitating conditions defined by $Re > 17,000$ – $19,000$ and $We > 3,500$ – $3,900$ and this is the only such study that was found where transitions from turbulent to cavitating flows were imaged, were comparable in macroscopic appearance to those of the current study and were at similar Re numbers. However, the current study indicates cavitation for all fuels well below the Re transition point for cavitation and for We numbers where hydraulic flip was reported in [29]. Furthermore, Ca values in [29] were in the range 1–4, whilst the current study shows cavitation at much larger Ca , with lowest range typically 12–18 for Nozzle B.

IMAGING ANALYSIS

This section presents and discusses images of cavitation and spray formation from the two optical nozzles over the range of fuels, temperatures and pressures used. It needs to be noted that although some of the features cannot be reproduced properly by the resolution of single images in hard copy format in the context of a printed publication, all the observations that will be presented and discussed were verified by close inspection and analysis of the respective high-speed movies.

Images of cold (20 °C) and hot (90 °C) gasoline injected into gas pressures of 1.0 and 0.5 bar are shown in Figure 15 for Nozzles A and B. The similar refractive index of the optical material and the fuels, in combination with the back light illumination method, allows the observation of cavitation inside the nozzle. Specifically, there is a dark flow region along the top of the nozzle passage at all conditions, indicating cavitation initiation at the flow separation point just at the nozzle's inlet. When the nozzle hole is completely filled with liquid fuel and light rays are incident at the nozzle hole perpendicularly, the area of total reflection at the transition boundary surface from the optical material to the fuel is kept at minimum [15]. On the contrary, when cavitation occurs in the nozzle, the presence of bubbles whose surface boundaries disperse the light rays makes cavitation areas appear as dark structures.

A close analysis of the images shows the dark cavitation region at the bottom of the nozzle passage extends upwards towards the nozzle's inlet with increase in temperature. One common feature of all the images is the asymmetric nature of the spray with the cone angle being greater at the top side of the spray plume on the nozzle side where cavitation occurs; the spray clearly experiences stronger break-up at the top, as also observed in [15, 16, 30, 31]. Collapsing cavitation bubbles outside injector nozzles is known to contribute to spray break-up and this seems to occur even at 20 °C. For hot conditions at the same gas pressure, it is likely that this collapse has an increased effect on the spray break-up as a result of different fluid properties *e.g.* lower surface tension, viscosity and higher vapour pressure, which all support faster bubble growth rates.

The lighter spray for hot conditions probably also indicates a higher concentration of vapour within the liquid fuel and/or higher concentration of fine droplets within the spray, as cavitation bubbles expand and burst rather than collapse, thus the ‘swelling’ seen in the primary break-up. These observations are compatible with similar plume swelling noticed in macroscopic imaging of the spray from the real multi-hole injector [21].

From gasoline’s images in Figure 15 it can be seen that at 20 °C the effect of a gas pressure reduction from 1.0 bar to 0.5 bar is relatively small. Although the gasoline spray is slightly wider at 0.5 bar gas pressure, the levels of cavitation inside the nozzle are comparable. It can also be observed that the in-nozzle cavitation pattern is different between the two nozzles at 20 °C fuel temperature. The cavitation film in Nozzle A with $d=0.5$ mm never reaches the bottom of the nozzle passage even when gas pressure is reduced from 1.0 bar to 0.5 bar. This does not happen to be the case for Nozzle B with $d=0.2$ mm. Here cavitation stretches down to the bottom of the nozzle passage at the outlet and extends to about a third of the nozzle length upstream of the outlet. However, both nozzles showed no significant change in cavitation structure when gas pressure was reduced from 1.0 bar to 0.5 bar.

At 90 °C fuel temperature and 1.0 bar gas pressure there is a slight increase in cavitation in Nozzle A, accompanied by an asymmetric increase in the spray cone angle. The cavitation in Nozzle B has expanded significantly upstream of the nozzle’s exit and occupies half to three quarters of the nozzle-hole passage, with a simultaneous increase in spray atomisation. The different cavitation patterns in the two nozzles are justified by the significantly different cavitation numbers in Figures 9–11. At 0.5 bar gas pressure and 90 °C fuel temperature, the spray cone angle is far greater than any of the other conditions and the fuel begins to atomise immediately outside the nozzle. The spray is still asymmetric with the top half angle of the spray plume larger than the bottom one (*i.e.* on the side of the nozzle where cavitation is present). The increased levels of flash-boiling at low gas pressures are also seen to reduce the dense dark area significantly and in fact within only 4–7 nozzle diameters the dark spray ‘core’ is no longer ‘intact’ and the backlight is clearly visible through the atomised spray. This is in clear contrast to the 1.0 bar gas condition which even at 90 °C shows a much narrower spray exiting the nozzle. A further interesting observation is that at 90 °C, gasoline’s in-nozzle cavitation at 1.0 bar gas pressure has extended upstream more than it has at 0.5 bar, particularly with Nozzle B. As will be shown later the same observation was made for all fuels at hot conditions, therefore, this is believed to be a real effect of the coupling between flash boiling and cavitation and the exact mechanism behind it requires further study with higher magnification.

The in-nozzle cavitation structure for E10 in Figure 15 appears to be similar at all conditions to that of gasoline except in the case of 90 °C fuel temperature and 0.5 bar gas pressure where the bottom dark corner of the nozzle-hole passage close to the nozzle exit appears longer for E10. Despite this difference, at 90 °C the in-nozzle cavitation pattern is seen to be longer at 1.0 bar than at 0.5 bar; this is a similar observation to that made for gasoline earlier. However, E10 sprays are more sensitive to operating conditions when compared to gasoline. The change in plume angle and atomisation when the gas pressure is reduced from 1.0 bar to 0.5 bar at 90 °C is greater for E10. This is also an indication that the level of superheating of the fuel

component has a higher effect on the rapid jet disintegration and atomisation than the level of cavitation in isolation since the in-nozzle cavitation structure between gasoline and E10 are not too dissimilar. The vapour pressure graph (Figure 7) and the fuel distillation curves (Figure 6) are helpful in analysing this behaviour. The vapour pressure of E10 is higher than that of gasoline and from the distillation curves one can further see that at about 80 °C, double the fuel has evaporated for the case of E10 in comparison to gasoline. This justifies the observations from the images which show that E10 is possibly flashing as soon as it is injected into the chamber at 90 °C and 0.5 bar gas pressure, thereby resulting in a larger cone angle and a more atomised spray in comparison to gasoline. At all other conditions, E10 exhibits larger areas of lighter ‘greyscales’ in the images that show up as larger ‘holes’ in the spray pattern with darker patches in-between.

Although the exact hierarchy of mechanisms is difficult to define because cavitation and flash-boiling remain highly coupled, it can be hypothesised that the process occurs as follows: upon release into the low gas pressure atmosphere, micro-bubbles originating from cavitation are acting as nucleation sites for the rest of the superheated components which increase the rate at which these can boil. This cascade process continues to the point where vaporisation can be nearly instantaneous. Bubble growth and the energy released from bubble rupture, which is transferred to the surrounding liquid, is therefore important in the production of new ligaments. In this respect, the surface tension is a critical parameter as it will define the surface energy necessary for bubbles to grow and break up the spray into smaller ligaments and droplets. The surface tension is generally lower and the viscosity is also lower for *n*-pentane and *iso*-octane in comparison to the heavy component *o*-xylene and to both ethanol and butanol discussed later, as indicated by the respective *We* and *Re* numbers throughout the studied range of fuel temperature; it is only at temperatures greater than ~120 °C (393 K) that ethanol’s *We* indicates better ability to atomise than *iso*-octane, whilst butanol shows always low ability to atomise similar to that of gasoline’s heavy component *o*-xylene. The mechanism can be further analysed when the relationship between cavitation and vapour pressure is considered. From the vapour pressure curves in Figure 7, it can be observed that under most of the conditions studied, the vapour pressure of gasoline, E10 and *n*-pentane was greater than the gas pressure. Cavitation inside the nozzle is governed mainly by the fuel temperature through its effect on vapour pressure, therefore, the relative difference between the vapour pressures at high temperatures and for a 0.5 bar change in gas pressure has a small effect. The effect of low gas pressure is demonstrated strongly outside the nozzle by two mechanisms; the first is the lower resistance to vapour-bubble growth and the second is the reduction of the liquid boiling point and automatic increase in the level of superheat experienced by the fuel constituents. This dramatically improves atomisation and destroys any remaining ‘solid core’ structure. The increased levels of superheat also drive the rapid evaporation process of the newly formed ligaments and droplets, so that fine atomisation can be nearly instantaneous.

In Figure 16 *iso*-octane appears relatively insensitive to operating conditions when compared to gasoline in Figure 15. At 20 °C there is no major difference in the spray produced, or in the mechanisms of primary break-up; the locations and levels of cavitation are also broadly similar. However, upon close inspection, it was clear that the cavitation ‘film’ in Nozzle A rarely reached the bottom wall of the hole, in contrast to gasoline’s behaviour in the same nozzle where even at 20 °C the cavitation film develops at the entrance of

the nozzle hole and extends to the bottom part of the passage, filling the hole fully at the nozzle exit plane. Cavitation in Nozzle B appears as a thinner film adjacent to the top wall of the nozzle-hole passage for both *iso*-octane and gasoline; in the case of Nozzle A cavitation is generally thicker from the inlet and increases more gradually as it expands downstream towards the nozzle's exit.

Reducing the gas pressure to 0.5 bar and maintaining the fuel temperature at 20 °C had no significant effect for *iso*-octane and only a small effect on the cone angle for gasoline. A rise in *iso*-octane's temperature to 50 °C showed almost no macroscopic differences to 20 °C, even for 0.5 bar gas pressure. However, there were some more obvious differences when the temperature was raised further from 50 °C to 90 °C. In Figure 16, cavitation at 90 °C has extended upstream of the nozzle exit and an increase in cone angle can be observed for Nozzle B, as the spray shows better atomisation. With a reduction in gas pressure at 90 °C, spray atomisation from Nozzle B is further enhanced as indicated by the lighter finer greyscales in the outer top region of the spray in the images. However, for Nozzle A, despite a change in cavitation broadly similar to that of Nozzle B, no significant change in spray formation can be observed as the spray can be seen to break-up similarly at the top and bottom with almost no obvious increase in the cone angle at the top. A comparison between images of *iso*-octane and gasoline gives a strong indication again that the levels of superheating of the fuel components contribute more towards the liquid jet's break-up and evaporation than the levels of cavitation in isolation, since cavitation structures are not very different between the two fuels over the full range of conditions but the sprays, particularly at 90 °C, are quite different indeed. Once again, it is observed that at 90 °C the dark cavitation region has extended upstream more at 1.0 bar gas pressure than at 0.5 bar, similarly for both nozzles; a similar observation was noted earlier for gasoline and E10.

Images of *n*-pentane sprays through Nozzles A and B are presented in Figure 17 for 90 °C. The sprays at 20 °C are not shown because these were not macroscopically very different to those formed by *iso*-octane and gasoline at the same temperature; a reduction in gas pressure from 1.0 bar to 0.5 bar at 20 °C showed no significant effect on the *n*-pentane spray, apart from a slight increase in the cone angle, as also observed for gasoline. The similarity between *n*-pentane and *iso*-octane sprays can be explained by the similar *We* number of these two fuels at 20 °C in Figure 12. The vapour pressure graph of Figure 7 indicated at first that the level of cavitation would be higher with *n*-pentane in comparison to *iso*-octane even at 20 °C because the vapour pressure of *n*-pentane at such low temperatures is similar to that of *iso*-octane at temperatures approaching 90 °C. The observed similarity in cavitation between the two fuels at 20 °C though can be understandable, when one also considers the relatively smaller overall effect of a raise in temperature from 20 °C to 50 °C and then to 90 °C on *iso*-octane's cavitation, in comparison to *n*-pentane's (the Cavitation number *Ca* of *n*-pentane in the region of 20 °C is also similar to that of *iso*-octane in the region of 70–90 °C).

By increasing the fuel temperature (with $p_g=0.5$ bar), similarities have been observed in the atomisation of *n*-pentane at 90 °C and gasoline in the range 90–120 °C from the real injector (*i.e.* at conditions of 'spray collapse', *e.g.* see [21]), although interestingly, cavitation is observed to be much less at 90 °C with gasoline in Figure 15 in comparison to *n*-pentane in Figure 17. This was also found to be the case when gasoline's temperature was briefly pushed to higher values than 90 °C with the optical nozzle, so that gasoline's spray

cone angle approached the wide cone angle of *n*-pentane at 90 °C. Moreover, work in progress has indicated similar droplet sizes between *n*-pentane and gasoline at these conditions [32]. Such observations can act as further evidence that, as a mechanism of atomisation enhancement, cavitation may not play as important a role compared to the levels of superheat experienced by the fuel components.

At 90 °C fuel temperature and 1.0 bar gas pressure, *n*-pentane shows excellent atomisation once again in Figure 17. However, the cone angle is smaller and there is some directionality in the spray. Differences in the spray formation should therefore stem from the lower levels of superheat as a result of the higher boiling point at 1.0 bar. It is also quite interesting that *n*-pentane showed macroscopically very similar atomisation characteristics to those at 90 °C and 1.0 bar when it was heated to only 50 °C but with gas pressure reduced to 0.5 bar. In-nozzle cavitation levels at 90 °C, 1.0 bar appear comparable to those at 90 °C, 0.5 bar, but with a slightly longer extension upstream towards the nozzle's inlet, as also typically observed with gasoline, E10 and *iso*-octane earlier.

Images obtained from the investigation of ethanol using Nozzle B are shown in Figure 18. In-nozzle cavitation appears similar at most conditions investigated, apart from 90 °C. Cavitation starts from the nozzle inlet and stretches all through to the nozzle outlet covering the top passage of the nozzle. Although the flow area covered by the dark cavitation region appears larger just close to the nozzle outlet, closer inspection showed that it never really touched the bottom side of the nozzle-hole passage for most conditions. In fact, the cavitation film appeared thinner than that observed with *iso*-octane at the same conditions. However, the spray break-up mechanisms appear slightly different over the studied range of conditions. At cold fuel temperature and atmospheric pressure, the spray appears asymmetric and breaks up more at the top, on the side where cavitation occurs in the nozzle. When gas pressure is reduced to 0.5 bar, while maintaining the fuel temperature at 20 °C, ethanol produces a slightly better atomised spray with more obvious ligaments on the side 'surface' of the spray, and an increase in cone angle, as can be justified by the thinner dark core in the spray when compared to the 1.0 bar gas pressure. No significant changes can be observed in both the in-nozzle cavitation and the spray break-up mechanism when ethanol is heated from 20 °C to 50 °C at atmospheric pressure. The increase in fuel temperature at sub-atmospheric pressure brings about some increase to the atomisation, with just a lighter appearance of the dark core. At 50 °C, the in-nozzle cavitation also appears slightly different between atmospheric and sub-atmospheric pressure. With 0.5 bar gas pressure, the dark cavitation region in the nozzle appears to be touching the bottom of the nozzle passage; this does not seem to be the case for 1.0 bar gas pressure.

At high temperatures, ethanol was found to react with the optical material of the nozzle resulting in some form of erosion to the nozzle-hole passage. Therefore, although at 90 °C cavitation occurs strongly inside the nozzle, it is difficult to give an informed description of its nature since the nozzle appears deformed at this condition, which in combination with ethanol's lower refractive index at this temperature, lowers confidence in drawing solid conclusions. Nevertheless, the cavitation pattern is clearly longer at 1.0 bar than at 0.5 bar, as also observed at hot conditions with the other fuels too. Additionally, it is clear that fuel atomisation increases strongly when the gas pressure is reduced to 0.5 bar at 90 °C fuel temperature, as justified by the

thin dark core and the wider cone angle of the spray. The case of 1.0 bar highlights further some of the complexities involved. Ethanol seems to behave quite different at 1.0 bar when compared to the 0.5 bar gas pressure case, as well as to the trends observed with the other fuels. While the other fuels experienced an increase in cone angle with temperature increase and pressure reduction, ethanol at 1.0 bar gas pressure underwent a gradual reduction in the dark region of its relatively compact spray. Whether this is related to the reaction between ethanol and the optical nozzle, or it is a true effect potentially due to supercavitation, remains unclear and needs further study with higher magnification and a nozzle of different grade or material.

For butanol sprays in Figure 19, the in-nozzle cavitation structure does not appear very different to that with ethanol, despite butanol's much lower vapour pressure; however, upon closer inspection it was observed that the cavitation film that extends from the nozzle passage's inlet to the outlet appeared slightly thinner for butanol. Another observation is that the dark cavitation region becomes greater towards the nozzle outlet but never touches the bottom of the passage, a similar behaviour to that of ethanol. Despite butanol's lower vapour pressure, the Ca of the two alcohols in Figure 9 is very similar at the same conditions, justifying to a degree the observed similarity in cavitation. Interestingly, butanol's Re number in Figure 8 at 20 °C also indicates flow very close to laminar conditions. Cavitation remains approximately the same when pressure is reduced to 0.5 bar at 20 °C and 50 °C in Figure 19. No significant differences in the break-up mechanism can be observed in all four conditions, though at 20 °C, the spray break-up at the top of the spray occurs earlier at sub-atmospheric pressure. In comparison to ethanol, at all these four conditions, butanol exhibits 'surface waves' with larger wavelength and a darker continuous core without as many 'holes' as ethanol. At 90 °C butanol undergoes an increase in spray atomisation but large ligaments and fuel blobs can be observed around the main spray. This was again a result of some deformation of the nozzle with the use of butanol and results cannot be confirmed as a typical representation of the fuel ability to cavitate and atomise at this temperature. Nevertheless, these have been included here for completeness and for relative comparison to ethanol's behaviour at the same temperature. The large fuel droplets that are showing up on the periphery of the butanol spray images are most probably a result of butanol's viscosity and surface tension (low Re and We) that restricts atomisation into as fine droplets as ethanol does at the same conditions (higher Re and We). Specifically, butanol's Re and We at 90 °C is similar to that of ethanol at 50 °C, with a respective similarity also at 50 °C and 20 °C (Figures 8 and 12). The trend of a longer cavitation core at 90 °C with gas pressure of 1.0 bar than with 0.5 bar is again apparent as with the all the other fuels discussed earlier.

SUMMARY AND CONCLUSIONS

This work investigated the effects of fuel temperature and gas pressure on cavitation and spray formation from a real-size optical nozzle. The nozzle was coupled to the body of a real multi-hole injector for DISI engines. Two nozzles were tested with nozzle-hole diameters of 0.5 mm (Nozzle A) and 0.2 mm (Nozzle B). Both nozzle holes were angled at 60° and the nozzle length to diameter ratio was kept fixed at a value of 5. All experiments were carried out in a quiescent pressure chamber for six fuels with different grades of volatility and for fuel temperatures 20 °C, 50 °C and 90 °C, and chamber gas pressures 0.5 bar and 1.0 bar.

These were conditions representative of in-cylinder thermodynamics for injection strategies during the early intake stroke of an engine for homogeneous mixture formation and for fuel temperatures over a range of typical engine-head temperatures. The tested fuels were of traditional and alternative type and included a commercial grade multi-component gasoline, the single components *iso*-octane, *n*-pentane, butanol, ethanol, as well as E10, *i.e.* a blend of 10% ethanol with 90% gasoline. The latter blend was tested because the vapour pressure of E10 is higher than the vapour pressure of either ethanol or gasoline and the distillation curve of E10 reflects strongly this effect. Therefore, distillation curves of the fuels, the vapour pressures, as well as density, viscosity and surface tension were obtained and the Reynolds, Weber, Ohnesorge and Cavitation numbers were considered in the study of the optical injector, with the Reynolds, Weber and Ohnesorge numbers set to match those of the real multi-hole injector. The in-nozzle flow regime was found to be highly sensitive to the fuel temperature as a result of the vapour-pressure and temperature relationships. Also, the degree of superheat experienced by the fuels outside the nozzle strongly improves primary break-up and spray atomisation. A reduction in chamber gas pressure brought about the widening of the spray plume signifying that higher gas pressures acts as a damping factor to the spray cone optimisation. This is mainly because of the effect of increased chamber gas pressure on the fuel vapour pressure or boiling point.

The main conclusions from this work can be summarised as follows:

- Cavitation was observed at all conditions and with both nozzles as a film on the top surface of the nozzles, indicating cavitation initiation at the flow separation point just at the nozzle's inlet. In general, cavitation in Nozzle B appeared as a thinner film adjacent to the top wall of the nozzle-hole passage with an abrupt change in width close to the nozzle's outlet; in the case of Nozzle A cavitation was generally thicker from the inlet and increased in width more gradually as it expanded downstream towards the nozzle's exit. The cavitation region became thicker and extended upwards towards the nozzle inlet with increased temperature but this did not always result in a geometric change in spray formation or faster spray break-up compared with cold conditions. The cavitation films appeared thinner with the two alcohols, particularly butanol, in comparison to the hydrocarbons. The lowest Cavitation numbers were in the range 12–18 for Nozzle B, whilst much larger numbers were calculated for Nozzle A. The relevant Reynolds numbers in the range 20–90 °C were 4,000–40,000.
- Analysis of the relationship between Ohnesorge and Reynolds numbers shows that *n*-pentane was generally in the atomisation regime when used with both nozzles but *iso*-octane was placed in the atomisation regime only with Nozzle B and crossed into the second wind induced regime when colder than ~70 °C (343 K) with Nozzle A. The two alcohols were placed in the second wind induced regime and cross into the atomisation regime only when at quite high temperatures and this is quite interesting in its own right considering the implications for engine cold-start conditions. Specifically, butanol crossed into the atomisation regime only when hotter than ~120 °C (393 K) and ~80 °C (353 K) with Nozzles A and B, respectively, whilst ethanol only when hotter than ~100 °C (373 K) and ~50 °C (323 K), respectively.

- One common feature in most of the spray images was the asymmetric nature of the spray with a greater cone angle at the top side of the spray plume, *i.e.* on the nozzle side where cavitation occurred. All fuels exhibited very similar cavitation patterns and atomisation at 20 °C despite the calculated Reynolds and Cavitation numbers predicting higher levels of in-nozzle cavitation for some fuels. The sprays at 90 °C, especially at 0.5 bar pressure were wider with ‘lighter’ cores indicating higher concentration of vapour within the liquid fuel and/or higher concentration of fine droplets within the spray, as cavitation bubbles expand and burst rather than collapse, thus the ‘swelling’ seen in the primary break-up.
- At high fuel temperatures, although the higher vapour pressures generally resulted in more cavitation inside the nozzle hole, it is the level of superheat, *i.e.* the extent to which the liquid temperature is above its boiling point at that gas pressure that determines the efficiency of atomisation. Cavitation is useful however because it supplies a plentiful source of vapour bubbles which act as nucleation sites to increase the rate at which superheated components in the spray can boil off. The biggest effect of gas pressure was in increasing/reducing the effective level of superheating experienced by the fuels through its effect on the boiling point.
- For gasoline an increase in fuel temperature increased the levels of in-nozzle cavitation and resulted in an asymmetric spray at both 0.5 bar and 1.0 bar gas pressures with the higher spray angle on the same side as cavitation in the nozzle. Spray break-up and atomisation efficiency were clearly improved.
- E10 behaved similarly to gasoline at all test conditions though with a slightly wider plume, except for the case of 90 °C fuel temperature and 0.5 bar gas pressure where the in-nozzle cavitation and atomisation was greater with E10. This was linked to the distillation curve of E10.
- For *iso*-octane an increase in fuel temperature caused an increase in the levels of in-nozzle cavitation with a relatively small increase in spray cone angle which did not significantly change the primary spray break-up even at 90 °C with Nozzle A. On the contrary, at the same conditions, Nozzle B showed both enhanced cavitation and atomisation.
- The in-nozzle cavitation was always greater for *n*-pentane compared to the other fuels which also was affected the most by the change in fuel temperature and gas pressure. At 90 °C fuel temperature an almost instantaneous vaporisation of *n*-pentane occurred outside the nozzle; this was further augmented with a reduction in gas pressure as the spray lost most of its directionality.
- For ethanol, an increase in liquid temperature from 20 °C to 50 °C did not cause much difference to the in-nozzle cavitation or the spray formation. At 90 °C, ethanol was found to react with the optical material and the nozzle appeared deformed, which in combination with ethanol’s low refractive index, precluded confident observation of the cavitation pattern. Additionally, although at 0.5 bar 90 °C ethanol’s atomisation appeared much improved, at the same temperature and 1.0 bar ethanol underwent a gradual reduction in the cone angle of the spray exhibiting a quite compact spray; it is not clear whether this was due to the deformation of the nozzle or supercavitation effects.

- For butanol, an increase in liquid temperature from 20 °C to 50 °C did not cause much difference to the in-nozzle cavitation or the spray formation. At 90 °C, butanol was also associated with some deformation of the nozzle which precluded confident observation of the cavitation pattern. However, at 90 °C ethanol's atomisation appeared much improved both at 0.5 bar and 1.0 bar. However, the sprays were accompanied by large droplets which surrounded the spray at elevated temperature.
- At 90 °C it was observed that all fuels exhibited longer in-nozzle cavitation patterns at 1.0 bar gas pressure than at 0.5 gas pressure. This was not accompanied with enhanced atomisation and required further study.
- Analysis of Cavitation numbers and images showed that gasoline is more temperature sensitive in comparison to *iso*-octane. Although *iso*-octane is commonly used as a substitute for gasoline in many engine research applications, higher volatility components, like *n*-pentane, are better substitutes for gasoline when a single-component fuel is to be used to model gasoline especially at elevated temperature conditions. This is particularly important to spray modellers who are normally faced with modelling a complete gasoline blend and have to make decisions on which single components might be more appropriate to use.

Current work is focused on studying the in-nozzle phenomena at higher magnification with a Questar[®] QM100 long-distance microscope and a pulsed laser illumination source to record the transient nature of cavitation. Since at high temperatures Perspex[®] was found to deform, especially when used with ethanol, new real-size optical nozzles are being manufactured from quartz in order to study reliably the full range of operation of DISI engine injectors with various fuels.

REFERENCES

1. Bergwerk, W., "Flow Pattern in Diesel Nozzle Spray Holes", Proceedings of IMechE, Vol. 173, No. 25, pp. 655–660, 1959.
2. Schmidt, D.P. and Corradini, M.L., "The Internal Flow of Diesel Fuel Injector Nozzles: A Review", International Journal of Engine Research, Vol. 2, pp. 1–22, 2001.
3. Serras-Pereira, J., Aleiferis, P.G., Richardson, D. and Wallace, S., "Mixture Formation and Combustion Variability in a Spray-Guided DISI Engine", SAE Transactions, Journal of Engines, Vol. 116, No. 3, 1332–1356, SAE Paper 2007-01-4033, 2007.
4. Aleiferis, P.G., Hardalupas, Y., Kolokotronis, D., Taylor, A.M.K.P. and Kimura, T., "Investigation of the Internal Flow Field of a Diesel Model Injector Using PIV and CFD", SAE Paper 2007-01-1897, 2007.
5. Walther, J., Schaller, J.K., Wirth, R., Tropea, C., Characterization of Cavitating Flow Fields in Transparent Diesel Injection Nozzles Using Fluorescent Particle Image Velocimetry (FPIV), Proceedings of ILASS-Europe, Darmstadt, Germany, 2000.
6. Walther, J., Schaller, J.K., Wirth, R. and Tropea, C., "Investigation of Internal Flow in Transparent Diesel Injection Nozzles using Fluorescent Particle Image Velocimetry (FPIV)", Proceedings of ICLASS, Pasadena, USA, 2000.

7. Arcoumanis, C., Flora, H., Gavaises, M. and Badami, M., “Cavitation in Real-Size Multi-Hole Diesel Injector Nozzles”, SAE Paper 2000-01-1249, 2000.
8. Soteriou, C., Andrews, R. and Smith, M., “Further Studies of Cavitation and Atomization in Diesel Injection”, SAE Paper 1999-01-1486, 1999.
9. Chaves, H., Knapp, M., Kubitzek, A., Obermeier, F. and Schneider, T., “Experimental Study of Cavitation in the Nozzle Hole of Diesel Injectors Using Transparent Nozzles”, SAE Paper 950290, 1995.
10. Aleiferis, P.G., Hardalupas, Y., Kolokotronis, D., Taylor, A.M.K.P., Arioka, A. and Saito, M., “Experimental Investigation of the Internal Flow Field of a Gasoline Model Injector Using Micro-PIV”, SAE Transactions, Journal of Fuels and Lubricants, Vol. 15, No. 4, pp. 597–606, Paper 2006-01-3374, 2006.
11. Allen, J. and Hargrave, G., “Fundamental Study of In-nozzle Fluid Flow and its Effect on Liquid Jet Break-up in Gasoline Direct Injectors”, Proceedings of ILASS-Europe, Darmstadt, Germany, 2000.
12. Allen, J., Hargrave, G.K. and Khoo, Y.C., “In-nozzle and Spray Diagnostic Techniques for Real Sized Pressure Swirl and Plain Orifice Gasoline Direct Injectors, SAE Paper 2003-01-3151, 2003.
13. Khoo, Y.C. and Hargrave, G.K., “Real-Sized Pressure Swirl GDI Injector Investigation with HSFV and FPIV”, Journal of Physics: Conference Series, Vol. 45, pp. 77–84, 2nd ICOLAD, 2006.
14. Moon, S., Bae, C., Abo-Serie E. and Choi, J., “Internal and Near-Nozzle Flow a Pressure-Swirl Atomiser under Varied Fuel Temperature”, Atomization and Sprays, Vol. 17, pp. 1–11, 2007.
15. Gilles-Birth, Bernhardt, S., Spicher, U. and Rechs, M., “A Study of the In-nozzle Flow Characteristics of Valve-Covered Orifice Nozzles for Gasoline Direct Injection”, SAE Paper 2005-01-3684, 2005.
16. Gilles-Birth, I., Rechs, M., Spicher, U. and Bernhardt, S., “Experimental Investigation of the In-nozzle Flow of Valve Covered Orifice Nozzles for Gasoline Direct Injection”, Proceedings of the 7th International Symposium on IC Diagnostics, pp. 59–78, Baden-Baden, Germany, 2006.
17. Balabin, R.M., Syunyaev, R.Z. and Karpov, S.A., “Quantitative Measurement of Ethanol Distribution over Fractions of Ethanol-Gasoline Fuel”, Energy and Fuels, Vol. 21, pp. 2460–2465, 2007.
18. Kar, K., Last, T., Haywood, C. and Raine, R.R., “Measurement of Vapour Pressures and Enthalpies of Vaporisation of Gasoline and Ethanol Blends and their Effects on Mixture Preparation in an SI Engine”, SAE Paper 2008-01-0317, 2008.
19. Serras-Pereira, J., Aleiferis, P.G., Richardson, D. and Wallace, S., “Spray Development, Flow Interactions and Wall Impingement in a Direct-Injection Spark-Ignition Engine”, SAE Paper 2007-01-2712, 2007.
20. Serras-Pereira, J., Aleiferis, P.G., Richardson, D. and Wallace, S., “Characteristics of Ethanol, Butanol, Iso-Octane and Gasoline Sprays and Combustion from a Multi-Hole Injector in a DISI Engine”, SAE International Journal of Fuels and Lubricants, Vol. 1, pp. 893–909, SAE Paper 2008-01-1591, 2008.
21. van Romunde, Z., Aleiferis, P.G., Cracknell, R.F. and Walmsley, H.L., “Effect of Fuel Properties on Spray Development from a Multi-Hole DISI Engine Injector”, SAE Transactions, Journal of Engines, Vol. 116, No. 3, pp. 1313–1331, SAE Paper 2007-01-4032, 2007.

22. van Romunde, Z. and Aleiferis, P.G. “Effect of Operating Conditions and Fuel Volatility on Development and Variability of Sprays from Gasoline Direct-Injection Multi-Hole Injectors” *Atomization and Sprays*, Vol. 19, pp. 207–234, 2009.
23. Aleiferis, P.G., Serras-Pereira, J., van Romunde, Z., Richardson, D., Wallace, S., Cracknell, R.F. and Walmsley, H.L., 2007, “Optical Studies of Spray Development in a Quiescent Chamber and in a Direct-Injection Spark-Ignition Engine”, *International Conference on Internal Combustion Engines: Performance, Fuel Economy and Emissions*, pp. 3–13, IMechE, London, UK.
24. Yaws, C.L., “Yaws’ Handbook of Thermodynamic and Physical Properties of Chemical Compounds”, Knovel, 2003.
25. Badock, C., Wirth, R., Fath, A. and Leipertz, A., “Investigation of Cavitation in Real Size Diesel Injection Nozzles”, *International Journal of Heat and Fluid Flow*, Vol. 20, pp. 538–544, 1999.
26. Ohnesorge, W., “Die Bildung von Tropfen an Dusen und die Auflösung Flüssiger Strahlen”, *Zeitschrift für Angewandte Mathematic und Mechanic*, Bd. 16, Heft 6, pp. 355–358, 1931.
27. Reitz, R.D. and Bracco, F.V., “Mechanisms of Atomization of a Liquid Jet”, *Physics of Fluids*, Vol. 25, pp. 1730–42, 1982.
28. Sallam, K.A., Dai, Z. and Faeth, G.M., “Liquid Break-up at the Surface of Turbulent Round Liquid Jets in Still Gases”, *International Journal of Multiphase Flow*, Vol. 28, pp. 427–449, 2002.
29. Suh, H.K. and Lee, C.S., “Effect of Cavitation in Nozzle Orifice on the Diesel Fuel Atomization Characteristics”, *International Journal of Heat and Fluid Flow*, Vol. 29, pp. 1001–1009, 2008.
30. Ganippa, L.C., Bark, G., Andersson, S. and Chomiak, J., “Comparison of Cavitation Phenomena in Transparent Scaled-up Single-hole Diesel Nozzles”, *CAV 2001*, Session A9.005, California, June 2001.
31. Hyun, K .S. and Chang, S .L., “Effect of Cavitation in Nozzle Orifice on the Diesel Fuel Atomization Characteristics”, *International Journal of Heat and Fluid Flow*, Vol. 29, pp. 1001–1009, 2008.
32. van Romunde, Z., “Factors Affecting the Development of Sprays Produced by Multi-Hole Injectors for Direct-Injection Engine Applications”, PhD Thesis, University College London, in preparation 2010.

LIST OF FIGURES

Figure 1. Pressure Chamber.

Figure 2. Schematic of Injector and Spray Plumes.

Figure 3. Optical Injector Assembly: (a) Injector in Mounting Plate, (b) Injector with Optical Nozzle in Mounting Plate, (c) Complete Injector Mount with Heater, (d) Optical Injector in Pressure Chamber.

Figure 4. CAD Drawings of Nozzle A ($d=0.5$ mm) and Nozzle B ($d=0.2$ mm); both nozzles at 60° to the vertical with $L/d=5$.

Figure 5. Experimental Setup.

Figure 6. Distillation Curves of Fuels Tested.

Figure 7. Vapour Pressure of Fuels Tested.

Figure 8. Reynolds Number with Nozzle A ($d=0.5$ mm) and Nozzle B ($d=0.2$ mm).

Figure 9. Cavitation Number (Ca) with Nozzle A ($d=0.5$ mm) and Nozzle B ($d=0.2$ mm).

Figure 10. Cavitation Number (CN) with Nozzle A ($d=0.5$ mm) and Nozzle B ($d=0.2$ mm), $p_g=0.5$ bar.

Figure 11. Cavitation Number (CN) with Nozzle A ($d=0.5$ mm) and Nozzle B ($d=0.2$ mm), $p_g=1.0$ bar.

Figure 12. Weber Number with Nozzle A ($d=0.5$ mm) and Nozzle B ($d=0.2$ mm).

Figure 13. Ohnesorge Number (Oh) with Nozzle A ($d=0.5$ mm) and Nozzle B ($d=0.2$ mm).

Figure 14. Ohnesorge Diagram with Nozzle A ($d=0.5$ mm) and Nozzle B ($d=0.2$ mm).

Figure 15. Gasoline and E10 Comparison with Nozzle A ($d=0.5$ mm) and Nozzle B ($d=0.2$ mm).

Figure 16. *Iso*-Octane Comparison with Nozzle A ($d=0.5$ mm) and Nozzle B ($d=0.2$ mm).

Figure 17. *n*-Pentane Comparison with Nozzle A ($d=0.5$ mm) and Nozzle B ($d=0.2$ mm).

Figure 18. Ethanol with Nozzle B ($d=0.5$ mm).

Figure 19. Butanol with Nozzle B ($d=0.2$ mm).

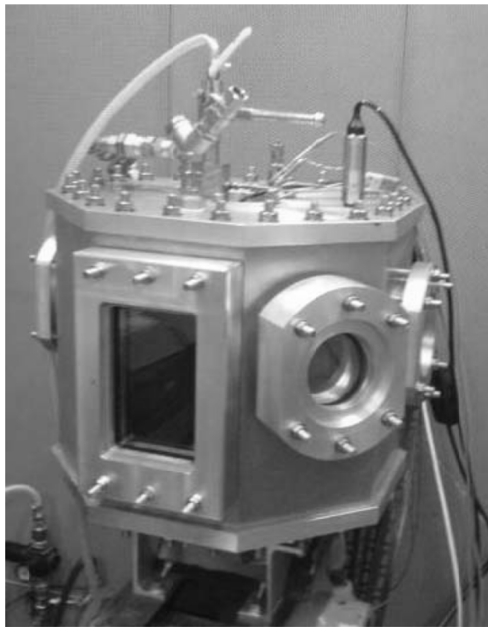


Figure 1. Pressure Chamber.

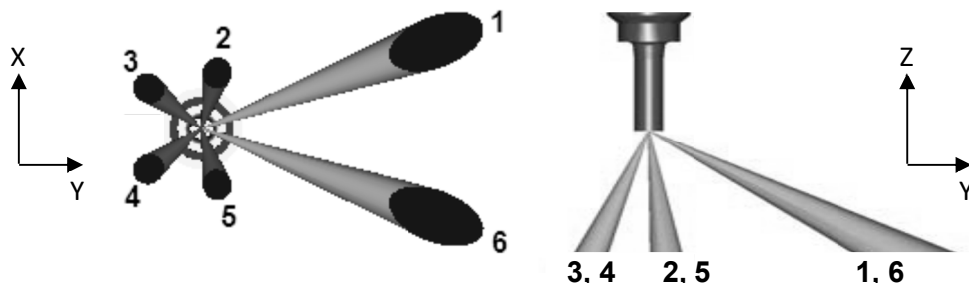


Figure 2. Schematic of Injector and Spray Plumes.

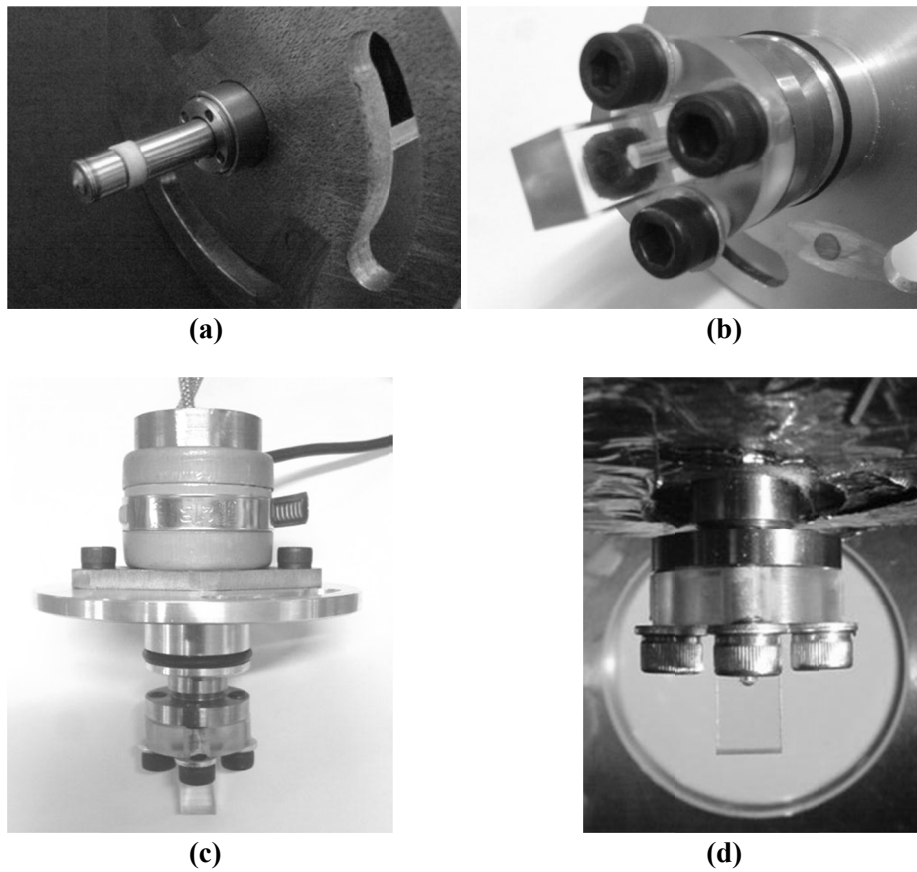


Figure 3. Optical Injector Assembly: (a) Injector in Mounting Plate, (b) Injector with Optical Nozzle in Mounting Plate, (c) Complete Injector Mount with Heater, (d) Optical Injector in Pressure Chamber.

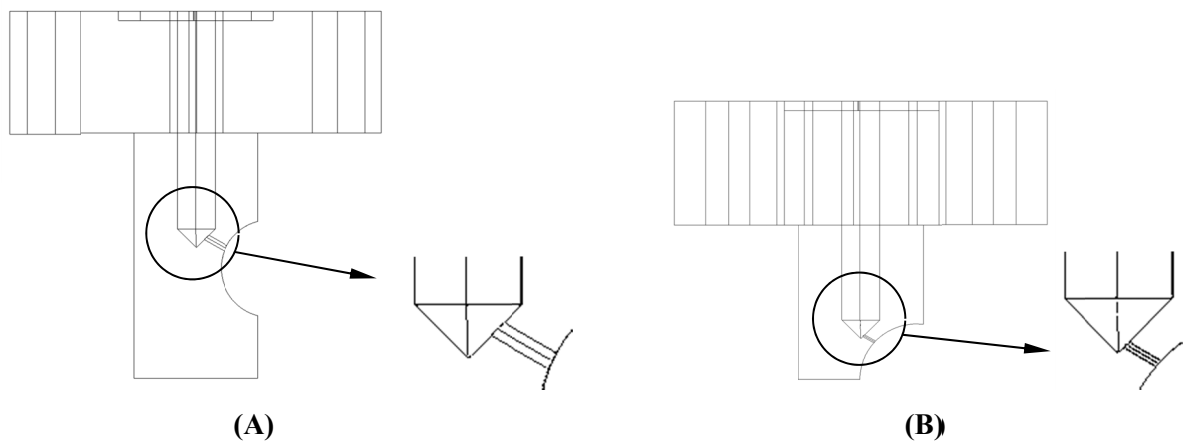


Figure 4. CAD Drawings of Nozzle A ($d=0.5$ mm) and Nozzle B ($d=0.2$ mm); both nozzles at 60° to the vertical with $L/d=5$.

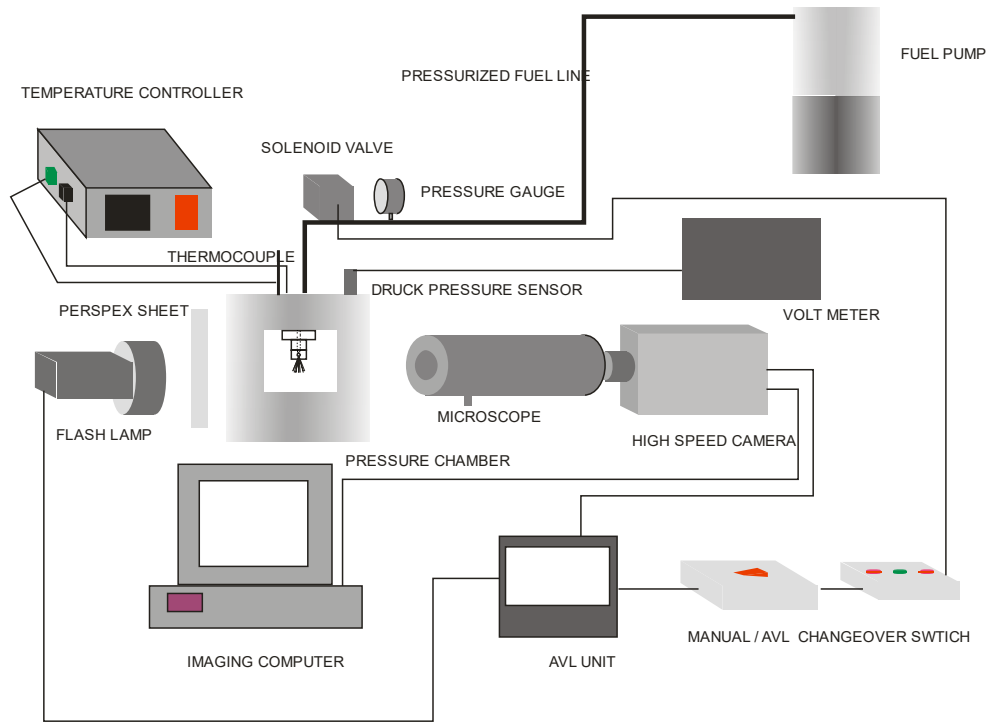


Figure 5. Experimental Setup.

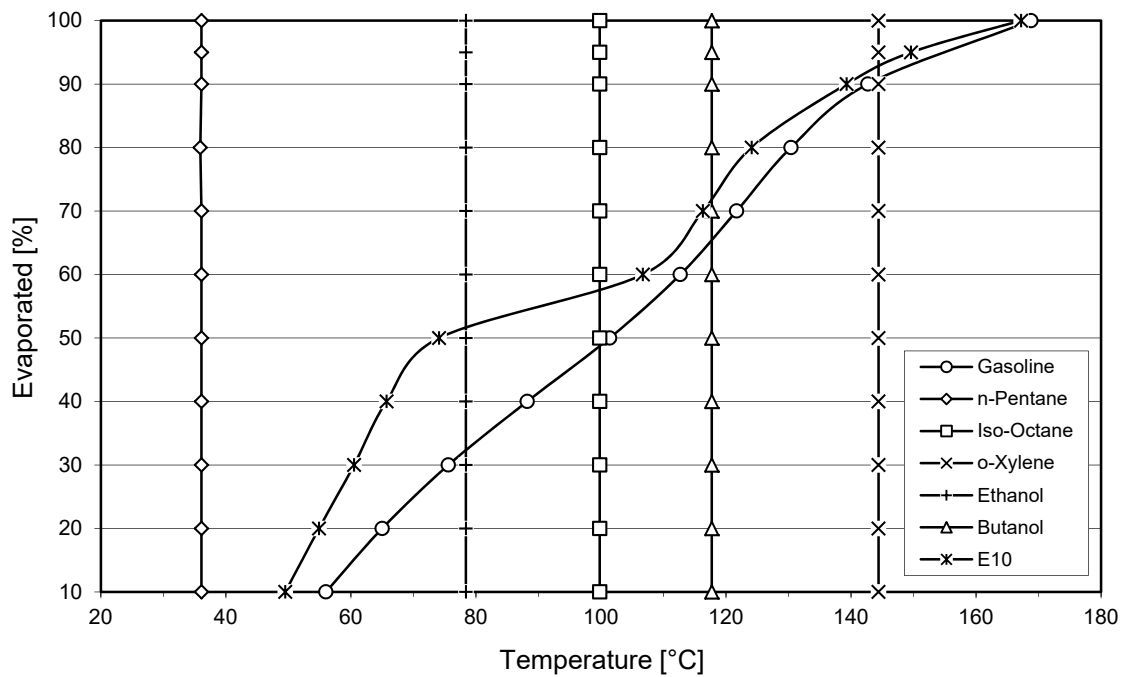


Figure 6. Distillation Curves of Fuels Tested.

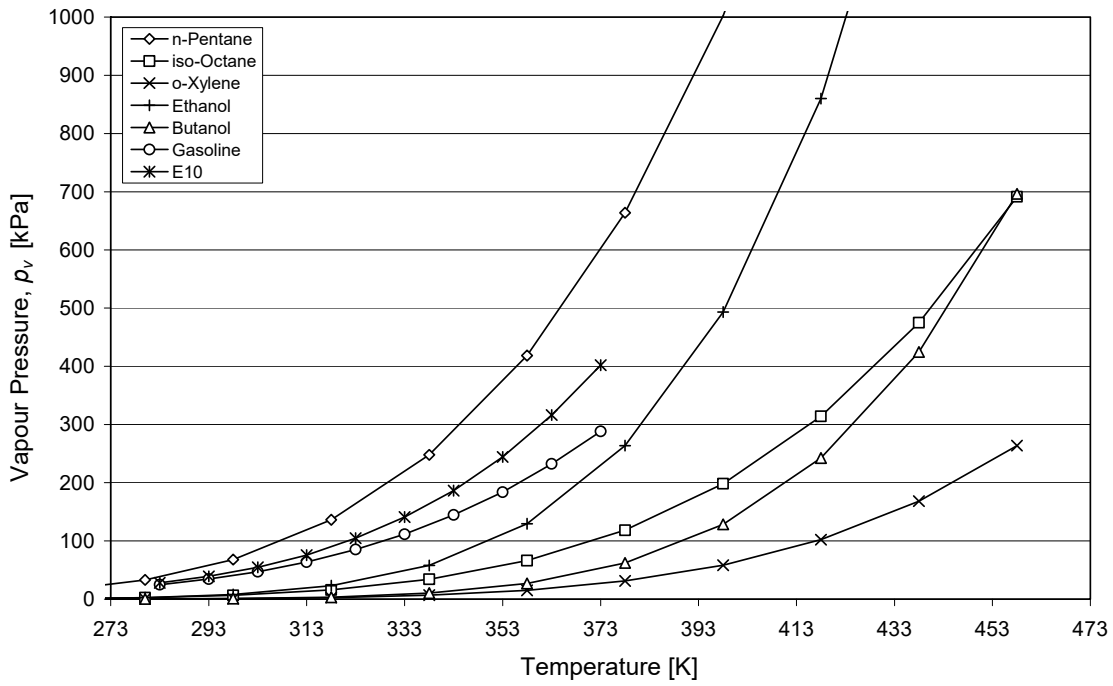


Figure 7. Vapour Pressure of Fuels Tested.

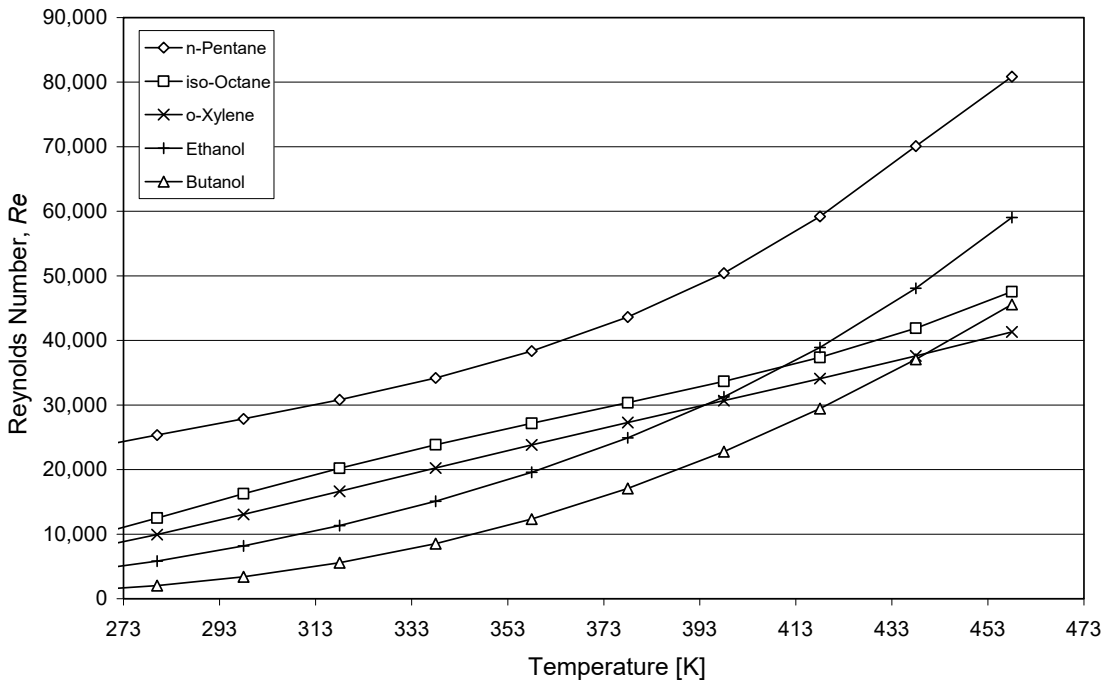


Figure 8. Reynolds Number with Nozzle A ($d=0.5$ mm) and Nozzle B ($d=0.2$ mm).

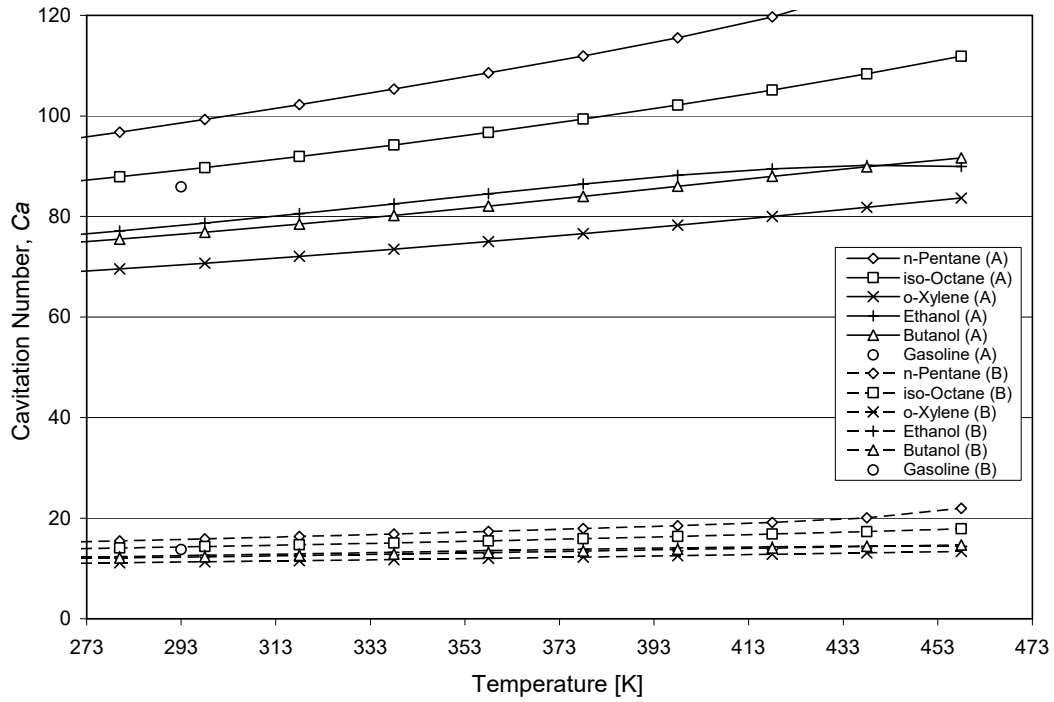


Figure 9. Cavitation Number (Ca) with Nozzle A ($d=0.5$ mm) and Nozzle B ($d=0.2$ mm).

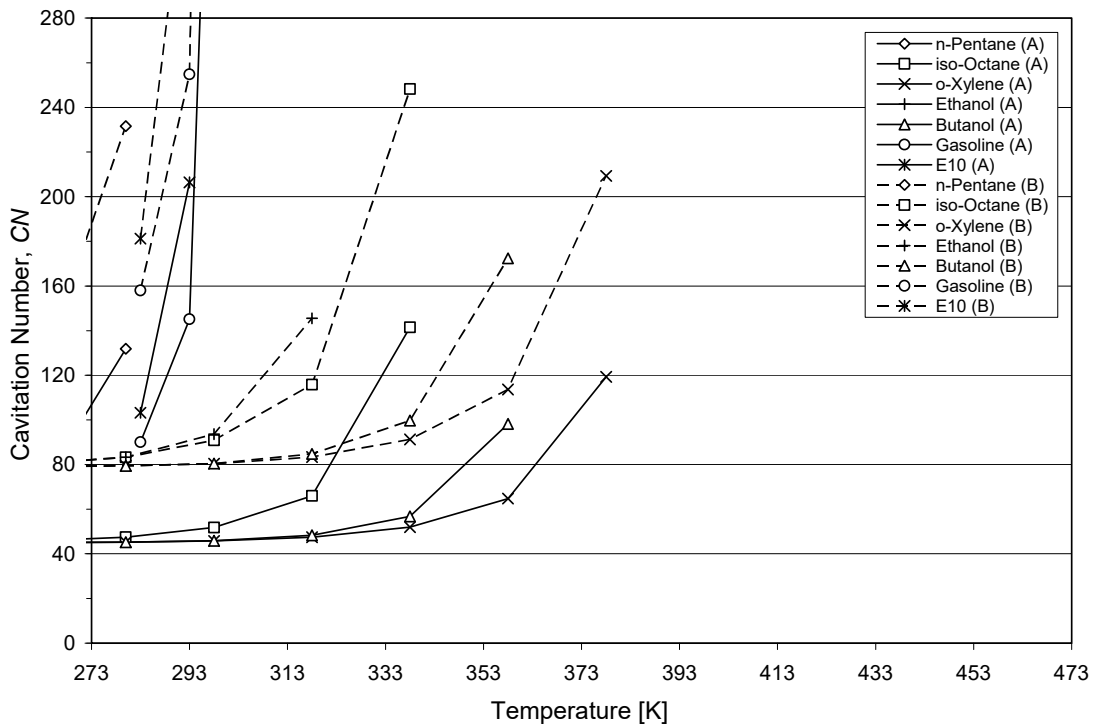


Figure 10. Cavitation Number (CN) with Nozzle A ($d=0.5$ mm) and Nozzle B ($d=0.2$ mm), $p_g=0.5$ bar.

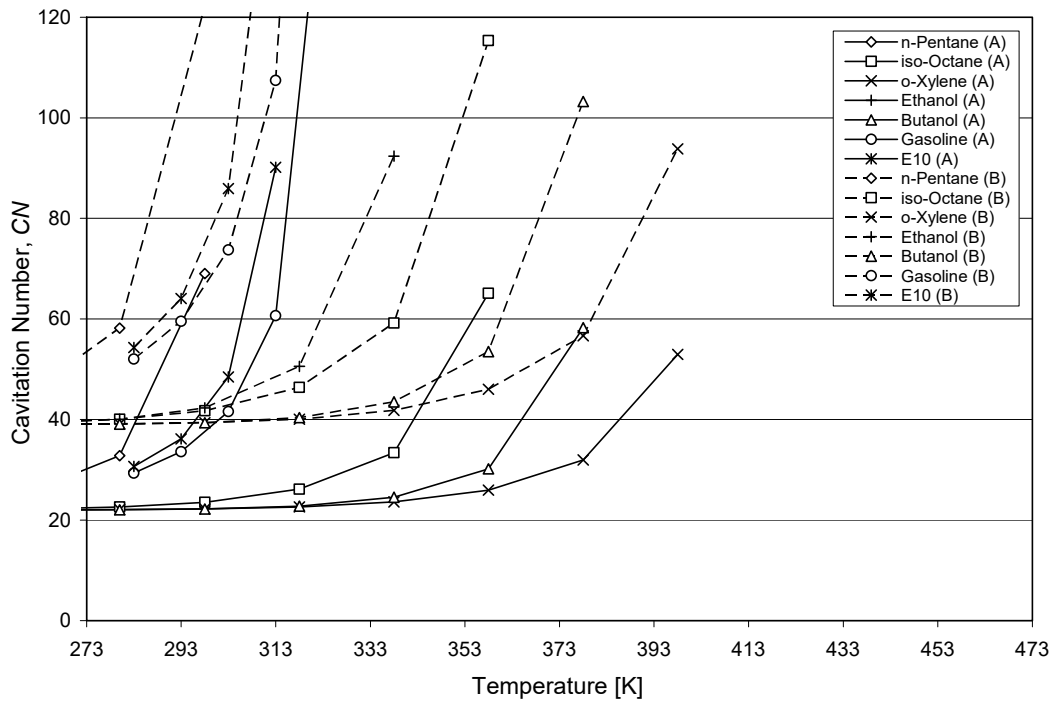


Figure 11. Cavitation Number (CN) with Nozzle A ($d=0.5$ mm) and Nozzle B ($d=0.2$ mm), $p_g=1.0$ bar.

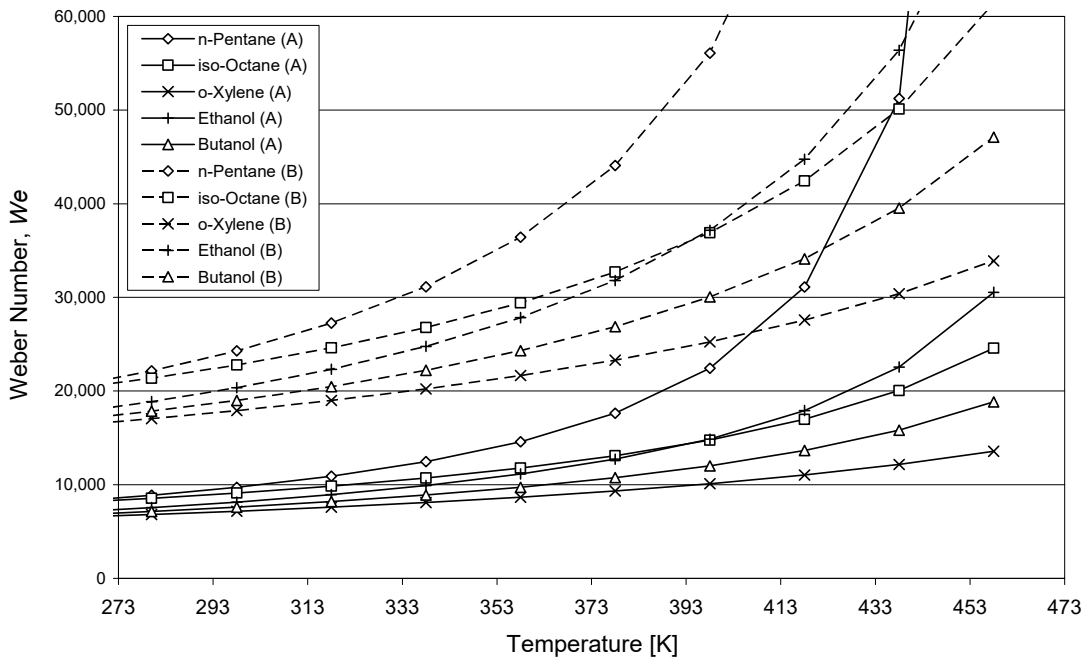


Figure 12. Weber Number with Nozzle A ($d=0.5$ mm) and Nozzle B ($d=0.2$ mm).

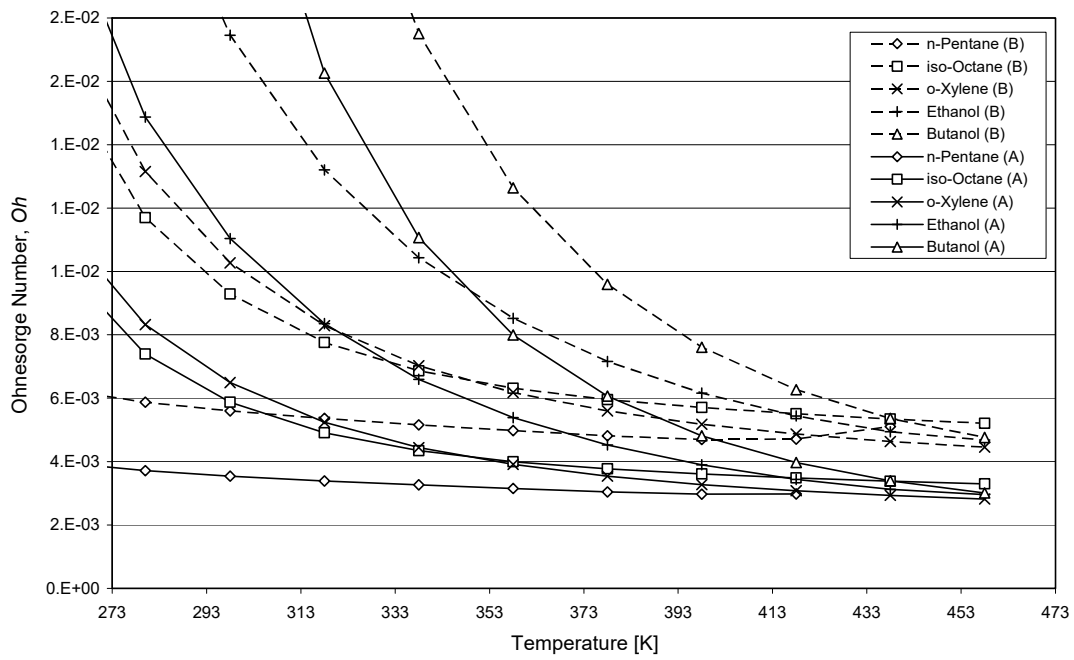


Figure 13. Ohnesorge Number (Oh) with Nozzle A ($d=0.5$ mm) and Nozzle B ($d=0.2$ mm).

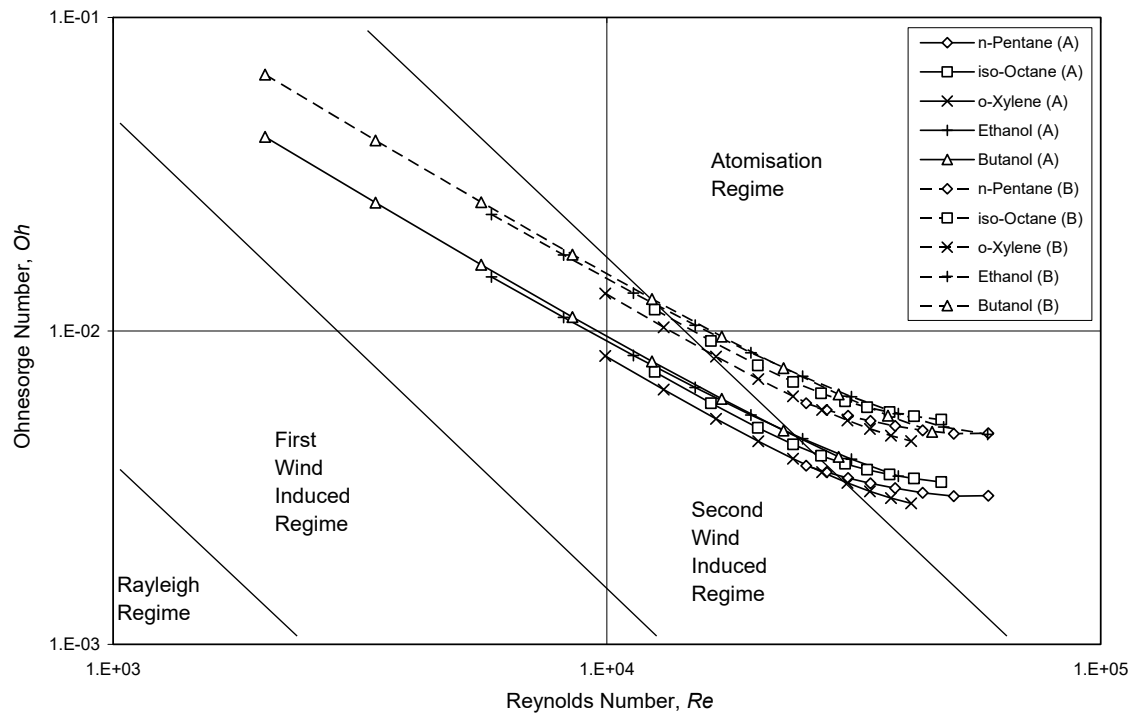


Figure 14. Ohnesorge Diagram with Nozzle A ($d=0.5$ mm) and Nozzle B ($d=0.2$ mm).

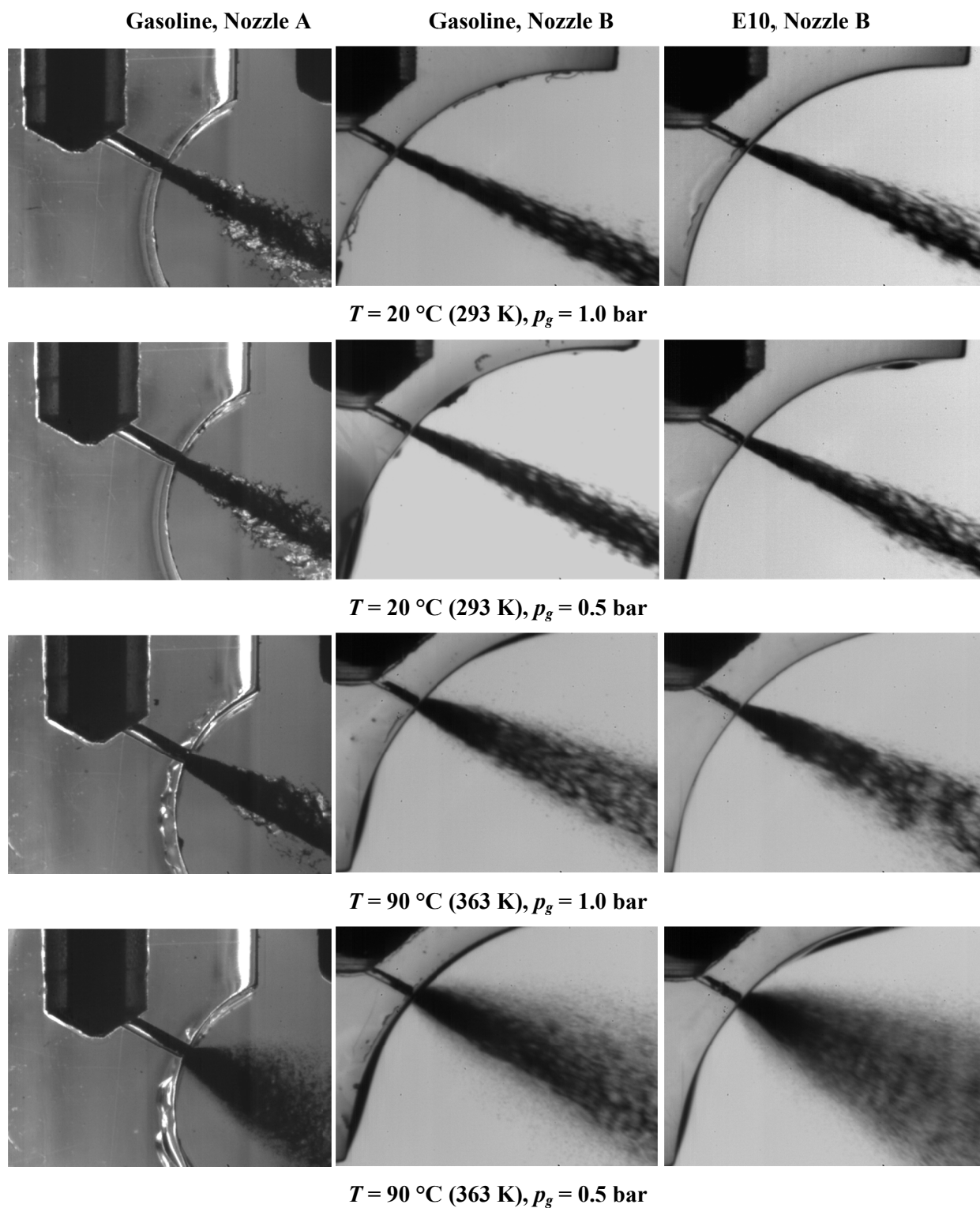
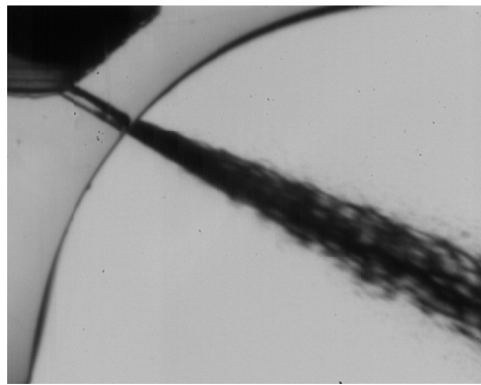
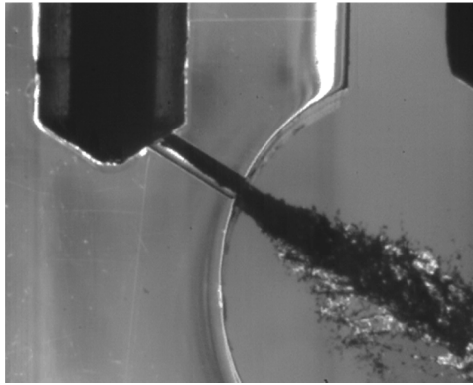


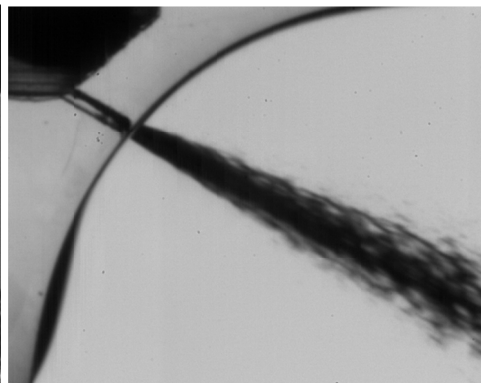
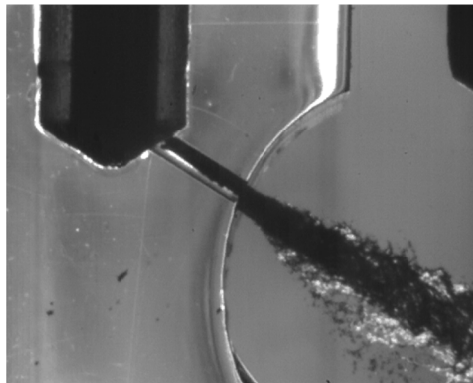
Figure 15. Gasoline and E10 Comparison with Nozzle A ($d=0.5\text{ mm}$) and Nozzle B ($d=0.2\text{ mm}$).

iso-Octane, Nozzle A

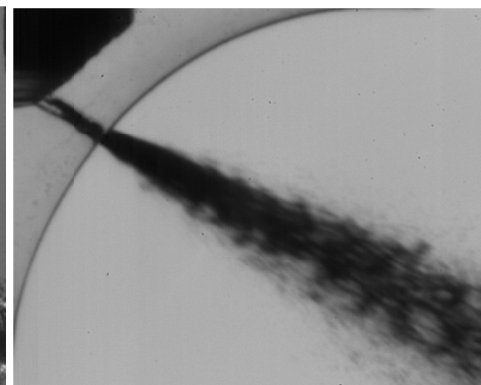
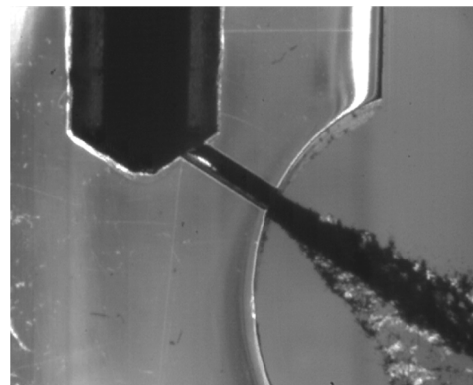
iso-Octane, Nozzle B



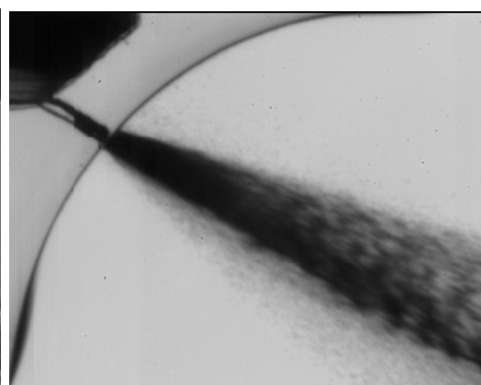
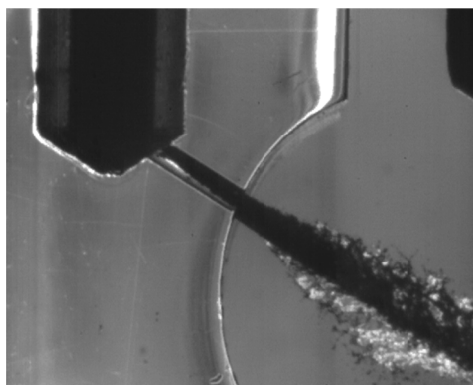
$T = 20\text{ }^{\circ}\text{C}$ (293 K), $p_g = 1.0\text{ bar}$



$T = 20\text{ }^{\circ}\text{C}$ (293 K), $p_g = 0.5\text{ bar}$



$T = 90\text{ }^{\circ}\text{C}$ (363 K), $p_g = 1.0\text{ bar}$

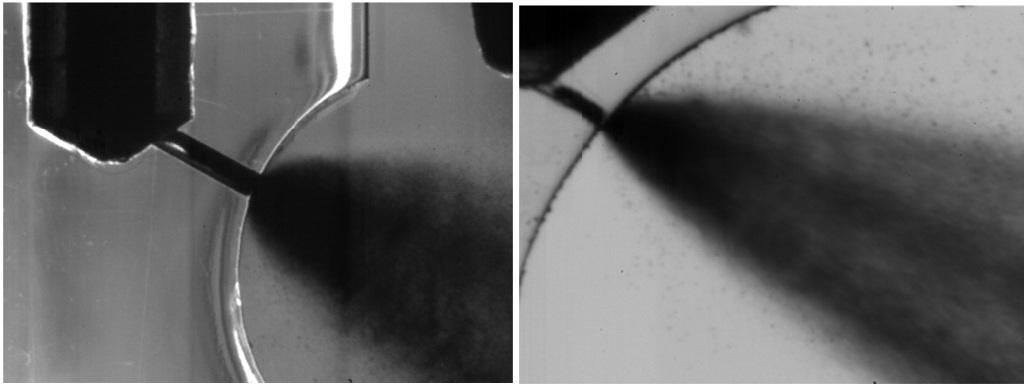


$T = 90\text{ }^{\circ}\text{C}$ (363 K), $p_g = 0.5\text{ bar}$

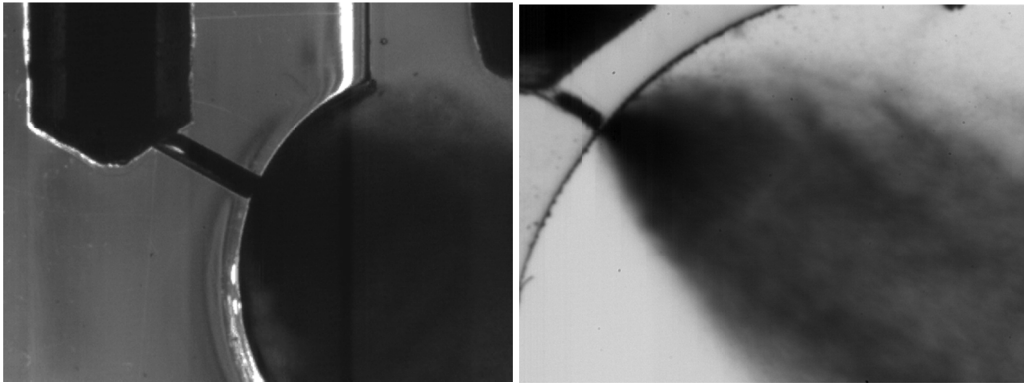
Figure 16. *iso*-Octane Comparison with Nozzle A ($d=0.5\text{ mm}$) and Nozzle B ($d=0.2\text{ mm}$).

n-Pentane, Nozzle A

n-Pentane, Nozzle B

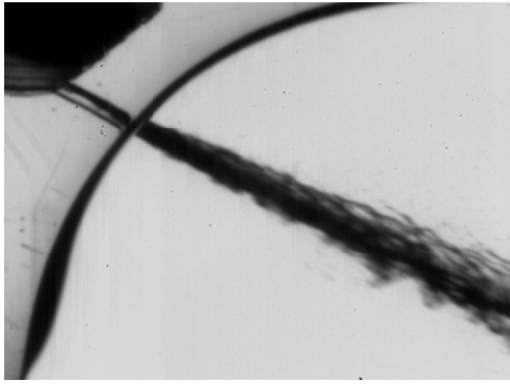


$T = 90\text{ °C (363 K)}, p_g = 1.0\text{ bar}$

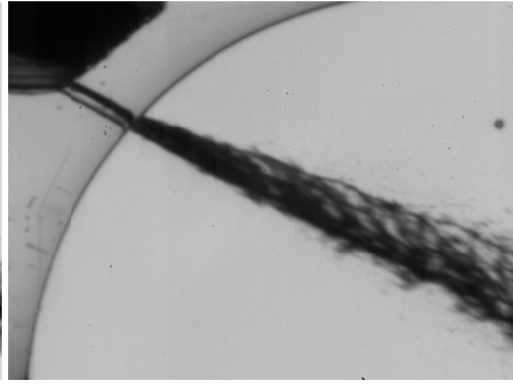


$T = 90\text{ °C (363 K)}, p_g = 0.5\text{ bar}$

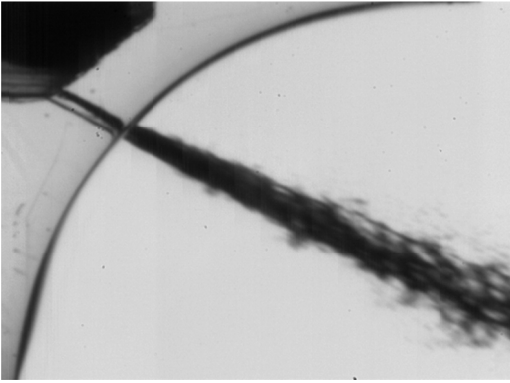
Figure 17. *n*-Pentane Comparison with Nozzle A ($d=0.5\text{ mm}$) and Nozzle B ($d=0.2\text{ mm}$).



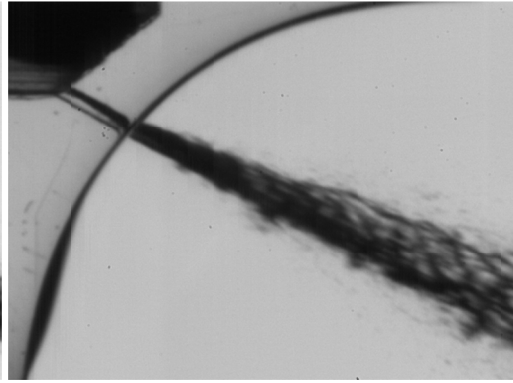
$T = 20\text{ }^{\circ}\text{C}$ (293 K), $p_g = 1.0\text{ bar}$



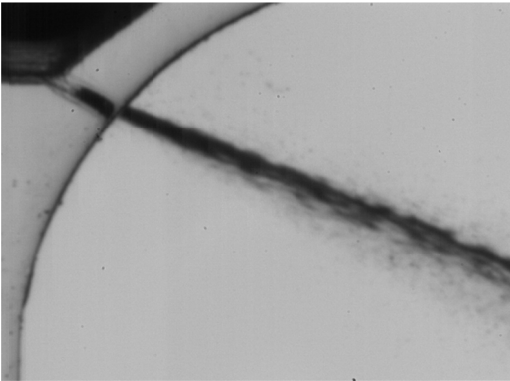
$T = 20\text{ }^{\circ}\text{C}$ (293 K), $p_g = 0.5\text{ bar}$



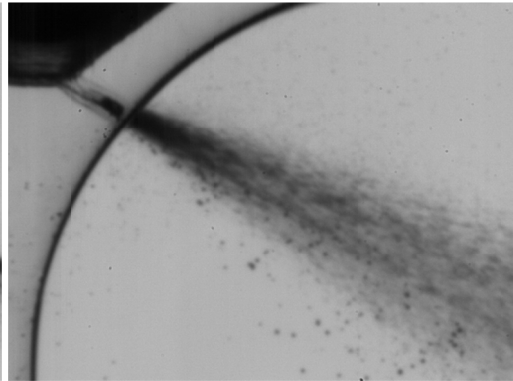
$T = 50\text{ }^{\circ}\text{C}$ (323 K), $p_g = 1.0\text{ bar}$



$T = 50\text{ }^{\circ}\text{C}$ (323 K), $p_g = 0.5\text{ bar}$



$T = 90\text{ }^{\circ}\text{C}$ (363 K), $p_g = 1.0\text{ bar}$



$T = 90\text{ }^{\circ}\text{C}$ (363 K), $p_g = 0.5\text{ bar}$

Figure 18. Ethanol with Nozzle B ($d=0.5\text{ mm}$).

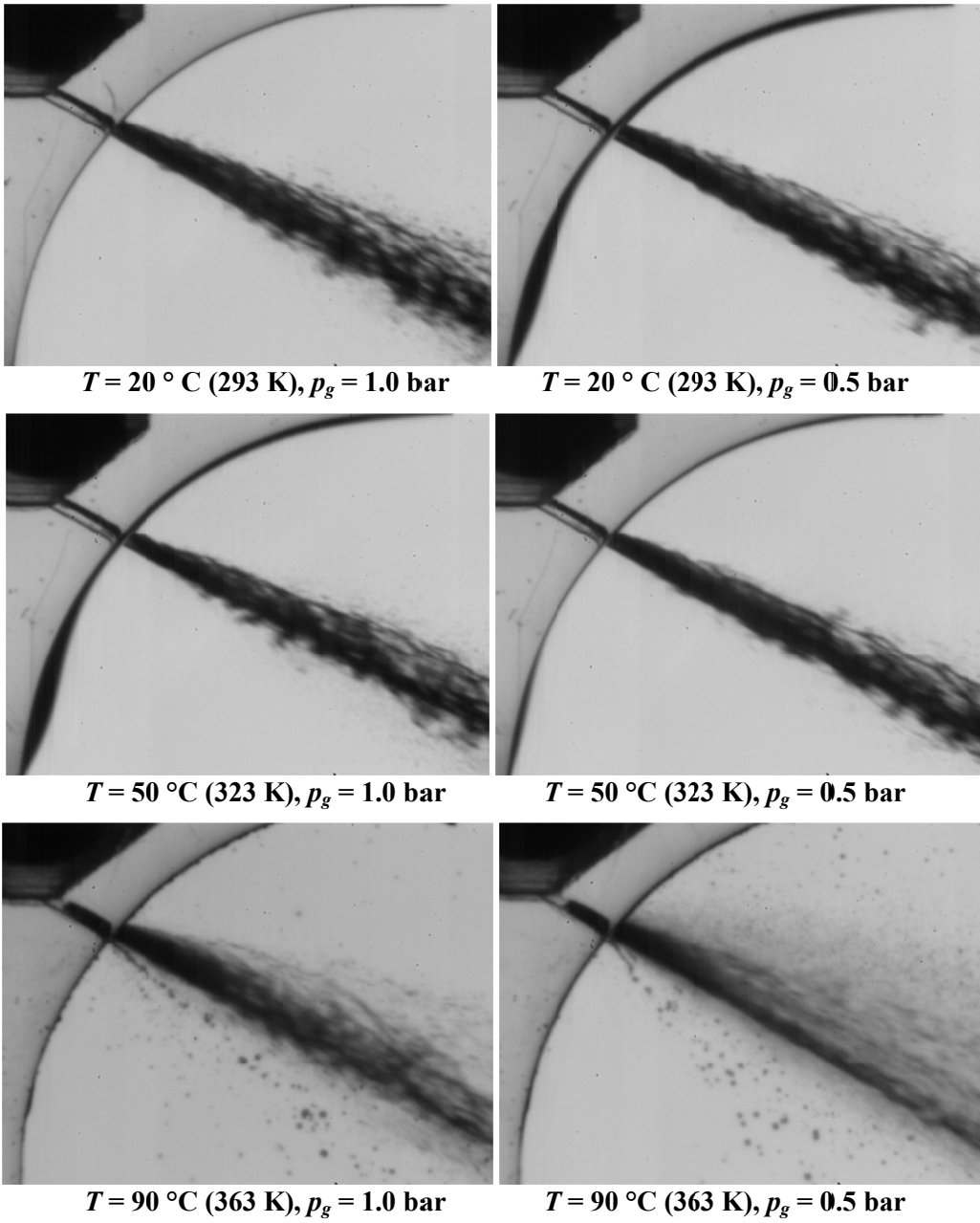


Figure 19. Butanol with Nozzle B ($d=0.2\text{ mm}$).